REPORT DOCUMENTATION PAGE

Form Approved
OMB No. 0704-0188

1. REPORT DATE *(DD-MM-YYYY)*	2. REPORT TYPE	3. DATES COVERED *(From - To)*
04/08/2020	Final Report	May 2018 - Jul 2020

4. TITLE AND SUBTITLE
Living Paint

5a. CONTRACT NUMBER
HR0011-18-9-0007

5b. GRANT NUMBER
N/A

5c. PROGRAM ELEMENT NUMBER
N/A

6. AUTHOR(S)
Gisser, Kathleen R.
Barton, Hazel A.
Rook, Tony

5d. PROJECT NUMBER
N/A

5e. TASK NUMBER
N/A

5f. WORK UNIT NUMBER
N/A

7. PERFORMING ORGANIZATION NAME(S) AND ADDRESS(ES)
The Sherwin-Williams Company
101 W. Prospect Avenue
Cleveland, OH 44115-1093

8. PERFORMING ORGANIZATION REPORT NUMBER
N/A

9. SPONSORING/MONITORING AGENCY NAME(S) AND ADDRESS(ES)
The Defense Advanced Research Projects Agency
675 North Randolph Street
Arlington, VA 22203-2114

10. SPONSOR/MONITOR'S ACRONYM(S)
DARPA

11. SPONSOR/MONITOR'S REPORT NUMBER(S)
N/A

12. DISTRIBUTION/AVAILABILITY STATEMENT
Distribution Statement A. Approved for public release; distribution unlimited

13. SUPPLEMENTARY NOTES
None

14. ABSTRACT
The Living Paint project investigated the ability of environmental and genetically-modified microbes to create a self-healing paint. Self-healing in damaged coatings was demonstrated using a previously unexplored calcium carbonate (CaCO3) biomineralization capability in microorganisms.

15. SUBJECT TERMS
Keywords: self-healing, microbes, microbially induced calcium carbonate precipitation, MICP

16. SECURITY CLASSIFICATION OF:			17. LIMITATION OF ABSTRACT	18. NUMBER OF PAGES	19a. NAME OF RESPONSIBLE PERSON
a. REPORT	b. ABSTRACT	c. THIS PAGE			Kathleen Gisser
					19b. TELEPHONE NUMBER *(Include area code)*
U	U	U	UU	38	216-566-2067

Living Paint

Kathleen R. Gisser[1], Hazel A. Barton[2], Tony Rook[1]

[1]The Sherwin-Williams Company, 101 W. Prospect Avenue, Cleveland, OH 44115-1093

[2]The University of Akron, 302 Buchtel Common, Akron, OH 44325-2102

This research was, in part, funded by the U.S. Government. The views and conclusions contained in this document are those of the authors and should not be interpreted as representing the official policies, either expressed or implied, of the U.S. Government.

Executive Summary

1.1 Project and Task Objectives

The *Living Paint* project investigated the ability of environmental and genetically-modified microbes to create a self-healing paint. The Sherwin-Williams Company, in partnership with the University of Akron, demonstrated self-healing in damaged coatings using a previously unexplored calcium carbonate ($CaCO_3$) biomineralization capability in microorganisms to create additional mass and volume at the site of the damage. This method allows self-healing without incurring mass-movement limitations of typical self-healing approaches. The long-term vision of this project is the complete synthesis of a composite coating from microbes and available natural resources.

Paints and coatings are designed to protect surfaces from damage. When the coating is scratched, gouged, abraded, or cracked, this compromises the coating and may reduce the overall performance of the system. Self-healing mechanisms for coatings have been studied for many years as a way to extend the life of a coating and reduce the maintenance costs associated with re-painting[i]. About 70% of architectural paint sold in the U.S. is white or light-colored and would be compatible with a $CaCO_3$ self-healing mechanism. A living paint would be a dual-use technology, as demonstrated by the U.S. Department of Defense's support for work in the area of self-healing coatings for asset protection (*e.g.*, ground vehicles, aircraft, and naval vessels).

The Base Phase task objectives focused on the development of materials capabilities. These objectives included an initial screen of nutrient and calcium type and location and the development of a coating material-based scaffold (Task 1), identification of the characteristics of an appropriate functional microbial species and down-selection to a pool of six candidates (Task 2), evaluation of genetic control to enhance calcium production and demonstration in a model *E. coli* system (Task 3), and determination of the robustness of candidate microbes to the type of coating (Task 4).

The Option Phase task objectives focused on system capabilities, including the delivery approaches for the microbes, water, calcium, nutrients, as well as activation and deactivation mechanisms. These objectives included exploring mechanisms to control growth and precipitation, while creating a healed area within 1 week that is roughly 10 x 1 x 0.25 mm^3, and approaches to create a system that did not require an agar underlayer (Task 5). The genetic control and hyper-expression system developed in Task 3 was translated into the functional bacterial species (Task 6). Paint performance testing of dried paint films was initiated to determine any loss of strength after repair (Task 7).

A successful system will deliver the following characteristics:

- Permanent repair of a damaged area in a model paint that is 10 x 1 x 0.25 mm^3;
- Repair that is visually opaque and able to obscure the original damage;
- Repair without the loss of strength of the original film;
- Minimal external intervention and maximized repair control (activation/deactivation).

1.2 Results

We have made substantial progress towards a successful system, demonstrating 10 x 1 x 0.25 mm^3 repair that is visually opaque. (Figure 29). The coatings were durable to standard washing tests (Figure 31) without causing uncontrolled microbial growth. Efforts to provide fully autonomous control of the

healing were less successful. All samples needed to be exposed to humidity and contact with an agar underlayer/primer layer to demonstrate a practical level of self-healing (Figure 14). However, we were able to demonstrate some microbial growth and calcification in samples in the absence of a support media (Figure 27, and Figure 28).

2 General methodology

***State-of-the-Art in Biomineralization*.** Microbial metabolic activity can change the chemistry of the microenvironment surrounding a cell and lead to altered physiochemical conditions that promote biomineralization.[i] Microbially-induced calcite precipitation (MICP) is one of the most studied mechanisms of biomineralization, with metabolic activities including photosynthesis, ureolysis, denitrification, ammonification, sulfate reduction, and methane oxidation all shown to induce the production of mineralized $CaCO_3$ (calcite).[ii] The three most common mechanisms for microbial product of calcite are photosynthesis, ureolysis, and calcium toxicity (Figure 1). It is likely that photosynthesis represents the most dominant mechanism for calcite biomineralization in the environment and may substantively contribute to the production of Earth's vast limestone deposits.[iii]

Figure 1. Mechanisms of biologically induced mineralization of calcite: A) Photosynthesis, B) Ureolysis, and C) Calcium toxicity enabled by ChaA antiporter (A), and the YadF carbonic anhydrase (F).

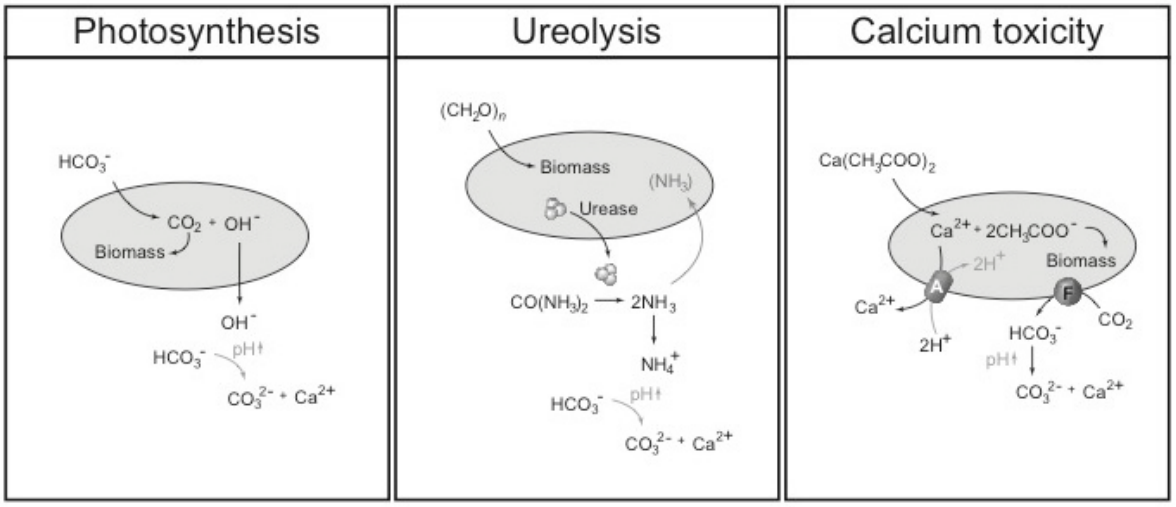

In the photosynthetic mechanism (Figure 1A), microbial CO_2 fixation increases the pH of the surrounding medium, exceeding the dissociation constant (pK_a) for HCO_3^-/H^+ favoring the formation of CO_3^{2-}. Available Ca^{2+} ions in seawater allow spontaneous calcification to occur. In the ureolytic mechanism bacteria produce the enzyme urease to catalyze the breakdown of urea to NH_3 and HCO_3^-. The NH_3 dissolves in water to form the NH_4^+ cation, which increases the local pH and (in a similar mechanism to photosynthesis) drives calcification. In the calcium toxicity mechanism, when the cell grows in calcium-rich environments, many organic compounds (such as glyoxylic acids) form a calcium salt (such as calcium acetate, Figure 1C). In order to grow on such calcium-rich organic compounds, the cell must have a detoxification strategy for toxic Ca^{2+} ions. The cell does this by pumping out excess calcium using the ChaA antiporter (A). When the extracellular levels of Ca^{2+} exceed the thermodynamic gradient of the transporter, the cell produces excess HCO^- ions from atmospheric CO_2 via the YadF carbonic anhydrase (F). A mutation in either c*haA* or y*adF* prevents the formation of calcite and is lethal in the presence of Ca^{2+} [iv].

To date, only ureolysis (Figure 1B) has been leveraged for biotechnological approaches, particularly for the biomineralization of self-healing concrete. In this approach, ureolytic bacteria catalyze the breakdown of urea to ammonium and bicarbonate ions.[v] Ammonium serves as a weak base to increase the local pH above the dissociation constant (pK_a) for HCO_3^-/H^+, driving the precipitation of carbonate ions. Ureolysis has several drawbacks, including malodor issues (from the production of ammonia), the limited distribution of naturally occurring ureolytic species, and the viability of ureolysis under extreme conditions, such as those found in concrete.[iii] The amount of organic carbon that must be embedded along with the bacteria to enable self-healing (up to 50 weight %) can dramatically reduce the tensile strength of the concrete itself.[vi] Despite these drawbacks, ureolysis has been one of the most extensively explored approaches for self-healing in engineered living materials.[iii]

Our past work in bacteria isolated from caves has demonstrated the ability of bacteria to excrete potentially toxic levels of Ca^{2+} using the ChaA transporter protein (Figure 1C). To overcome the thermodynamic barrier against pumping out Ca^{2+}, the cell modifies the extracellular environment through buffering with HCO_3^- which alters the pH and leads to the spontaneous precipitation of $CaCO_3$. In our past work, we identified over 50 strains that were precipitators of $CaCO_3$ as calcite. For the Living Paint project we started with the spore formers P6A (*Bacillus simplex*) and P12B (*Bacillus subtilis*), which were compatible with several latex binders, and continued to screen microbes for inclusion in our pool during Task 2.

State-of-the-Art in Coatings and Self-Healing approaches. Paints and coatings are generally comprised of a polymeric binder that serves as glue; pigments such as calcium carbonate, titanium dioxide, or silicate clays to enhance durability and add opacity; and a solvent (water or organic) that serves as a carrier. A variety of functional additives are used to provide rheology control, shelf-stability, and other features. The model coatings developed for the current project are described in the experimental section of Task 1.

Current extrinsic self-healing technologies for such coatings require temporary local mobility of material and are generally based on either of two approaches. The first involves the incorporation of a healing payload in capsules that, when broken, flows to fill the damage. The second uses a more complicated vascular, tube, or channel structure that allows the flow of material to fill cracks in the damaged coating when activated. The shortcoming of these approaches is that they are based on the movement of material within the coating. Before the damage, the coating is weakened by the inclusion of up to 20 weight percent unreacted material. After self-healing, the voids that are created can also weaken the coating. Intrinsic self-healing coatings based on flow are generally solvent-borne clear coatings and require heating to actuate. If material is removed from an intrinsic self-healing coating, it is not available to flow.

3 Technical Problems, Results, Important Findings and Conclusions for Tasks 1-7. (*Tasks are re-ordered to enhance readability*).

3.1 Initial screen of Materials Capabilities. (Task 1).

3.1.1 Technical Problems

The creation of a self-healing coating required the development of several materials capabilities. These include appropriate nutrients, calcium sources, moisture, and the coating system in which the microbes reside. In addition, a scaffold replacement for the agar underlayer was explored. In the proof-of-

Table 1. Materials Capabilities

Material Capabilities Investigated in Task 1	
Capability	**Approach**
Nutrient type	Complex, Defined, Inducible
Calcium type & delivery	Particulate, Organic salt, Inorganic
Water delivery	Growth media, humidity, liquid application
Protection from coating materials	Sporulation (Gram Positive), encapsulation (Gram negative)
Coating and Scaffold materials	Coating / Agar scaffold Coating / Coating scaffold Coating, no scaffold Additional coating chemistries

concept work preceding this project, an agar scaffold provided a source of moisture (which is incorporated in the gel structure), a way for the microbes to move to the site of damage, and the opportunity for spatial segregation of nutrients. In this task, we identified potential coating material scaffolds based on porosity and hydrophobicity to enable motility and hold moisture. An initial assessment of these approaches was also carried out.

The key materials capabilities that were developed for the project are described in Table 1, along with the approaches investigated in Task 1 of the Base Phase. Task 1 involved initial screening experiments. As approaches were explored and discarded a subset of these materials were used in Task 5, where we attempted to build more optimized systems.

3.1.2 Technical Results

Nutrients. We first evaluated non-selective nutrients (tryptic soy broth, TSB), either superficially, within the coatings or within the agar scaffold. The addition of TSB at many of these locations resulted in both microbial growth and calcification. Non-selective nutrients were compatible with the binders and coatings. Because this approach was successful, we did not pursue further work with complex or selective nutrients in our initial screening.

Calcium type and location. Microbially induced carbonate precipitation (MICP) is frequently assessed through the use of B4 Media. Standard B4 media contains 4 g yeast extract, 10 g glucose, and 15 g agar per liter of media [vii]. The media is adjusted to pH 7.2 before autoclaving. Calcium acetate is used as the calcium source, dissolved in water and filter-sterilized before addition to the media following autoclaving. Following autoclaving, the B4 media and filtered calcium acetate are typically kept separated until needed to prevent precipitation of the calcium source. In this work, minimal B4 media was also used, omitting the glucose from the formula.

Eight calcium salts, including organic and inorganic salts, were evaluated as additives to growth media instead of calcium acetate. Many of them were able to supply calcium ion to the microbes and resulted in the precipitation of calcium carbonate, although microbes grown with different calcium salts produced different amounts of calcium carbonate.

The initial assessment of the impact of the calcium salts on calcification was followed with a more detailed study with the wild type *E. coli* used as the model organism for the genetic work in Task 3. Neither *E. coli* K12 nor any of the species in the Keio gene knockout library (Baba et al., 2006), demonstrated a calcification phenotype on B4 media. Nonetheless, in previous work we demonstrated that *E. coli* produces a number of organic acids when grown in the presence of glucose, which are produced through a combination of metabolic overflow, acetogenesis, and mixed acid fermentation. As $CaCO_3$ precipitation is directly related to the pH and saturation index, we wondered if the inability of these *E. coli* strains to calcify on B4 was due to acidification of the media. To test this, we set up cultures in B4 without the addition of glucose, which led to an increase in media pH (>8.8) and calcification. Given that *E. coli* can grow on a number of other calcium salts beyond calcium acetate (calcium propionate, calcium lactate, calcium pyruvate, and calcium succinate) we demonstrated calcification on B4 media where calcium acetate was substituted for these calcium salts, and demonstrated calcification in all the media. As a control, we used calcium citrate. The CitT transporter is only induced under anaerobic conditions, and while *E. coli* grew on calcium citrate media and produced alkali conditions, the lack of calcification demonstrates the importance of a metabolizable calcium salt in promoting calcification. This modified media allowed us to use *E. coli* as a model organism to screen a number of metabolic properties for their influence on calcification, including screening the Keio library to examine other genes that may play an important role.

$CaCO_3$ (which is typically included in paint formulas) was of interest as a source of calcium ions for self-healing. There is evidence (see Figure 22 below) that an organic calcium salt is not necessary for calcification to proceed. There appears to be enough calcium in our model coatings to drive calcification**.** The location of the calcium source was investigated by incubating model paint coupons with P6A and P12B on media with no additional calcium source in the growth media, meaning that the sole source of calcium for mineralization came directly from the model paint. The micrograph below shows the result of incubating model paint coupons with P12B on media lacking calcium sources. Dark areas show calcification. There is evidence of calcification in the coating, as well as calcification outside the coating, that is beginning to bridge the cracked area of the film.

We examined different locations for $CaCO_3$, both in the paint film and in a segregated scaffold distinct from the location of the bacteria. In both cases, this allowed calcification.

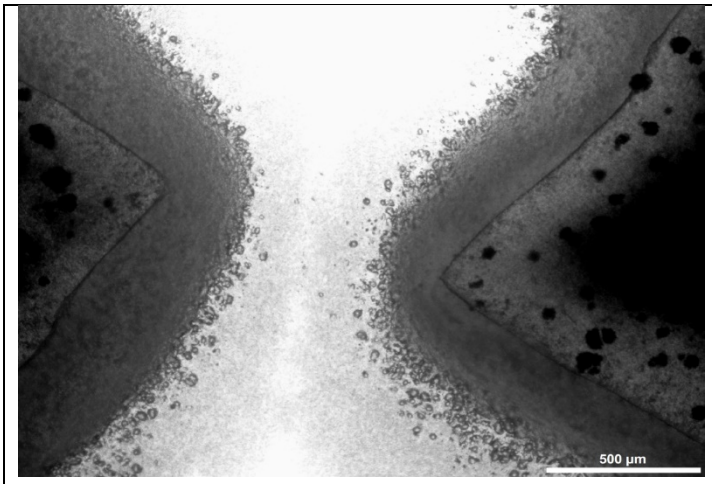

Figure 2. Microbial Growth and Calcification. Micrograph of a model paint formula with P12B that was incubated on media containing no calcium (the only calcium source was from the model paint formula).

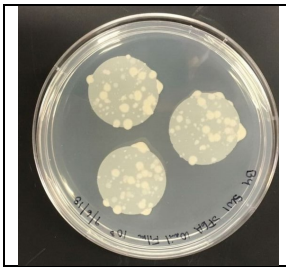

Figure 3. Dry paint coupons on an agar scaffold show microbial growth and calcification.

Inducer chemistry: The initial work with plasmids (Task 3) focused on pPro, which allows for induction with propionate. In preparation for the genetics work, we determined that the addition of calcium propionate at 13.4 mM did not affect the ability to mix or make films from the resulting model paint.

Water delivery. We evaluated three mechanisms of water delivery: contact with hydrated growth media, atmospheric humidity, and direct application. Early experiments with dried paint coupons in contact with growth media successfully demonstrated microbial growth and calcification, typically at the edges of the coupons, in addition to the face of the coupons.

Without the growth media, incubating the coupons at 90% relative humidity alone did not induce growth. Coupons with a coating scaffold to replace the agar growth media also did not show any microbial growth when exposed to 90% humidity. However, wetting the coupons with liquid water or nutrient broth (TSB) initiated growth and some calcification, as described in the experiments below.

Sporulation protocols were developed for P6A (*Bacillus subtilis* control species) grown in TSB for 9 days. The mixed cell/spore suspension was pelleted at 2,700 x g for 10 min in a centrifuge and resuspended in 25 mL sterile H_2O with shaking for an additional 7 days. The P6A and P12B strains could be induced to obtain >99% sporulation, allowing spore purification and removal of vegetative cells.

When added to the paint and drawn down into a film, scanning electron microscopy (SEM) indicated that the spores tend to clump together. Initial Zeta potential studies indicated that distribution may be linked to the charge on the spores themselves.

Figure 4. SEM images of spores dispersed in a model paint that was cast into a film. The left-hand image is looking down on the surface and on the right is a close up from a cross-section. The spores appear to be present in small (5 micron) agglomerates of 10 to 20 primary particles.

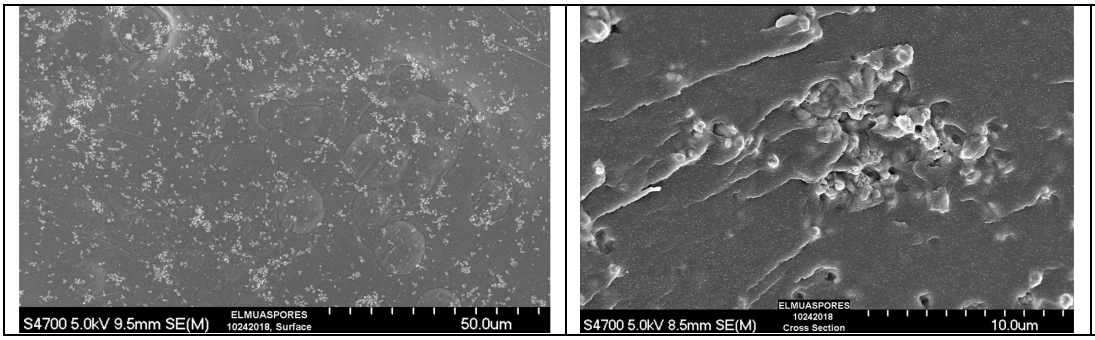

Encapsulation. Since we desired to evaluate non-spore formers in the Option Phase, an encapsulation procedure was developed in alginates based on Sheu et al., 1993.[viii] An environmental *Comamonas* (Comamonas *1)* was successfully encapsulated and was tested for survival in paints as part of Task 2. We were able to encapsulate bacteria in alginate capsules, with capsule sizes ranging from 5 - 100

microns, which enhanced the survival through the use of charged particles.

Figure 5. Alginate capsules containing *Comamonas 1*. A) Alginate capsules containing *Comamonas 1* cells (grey inclusions); B) Alginate capsules with charged particles. The *Comamona 1s* cells seemed to clump towards the particles and showed an increased survival for up to 1 month. In both images the scale bar is 10 microns.

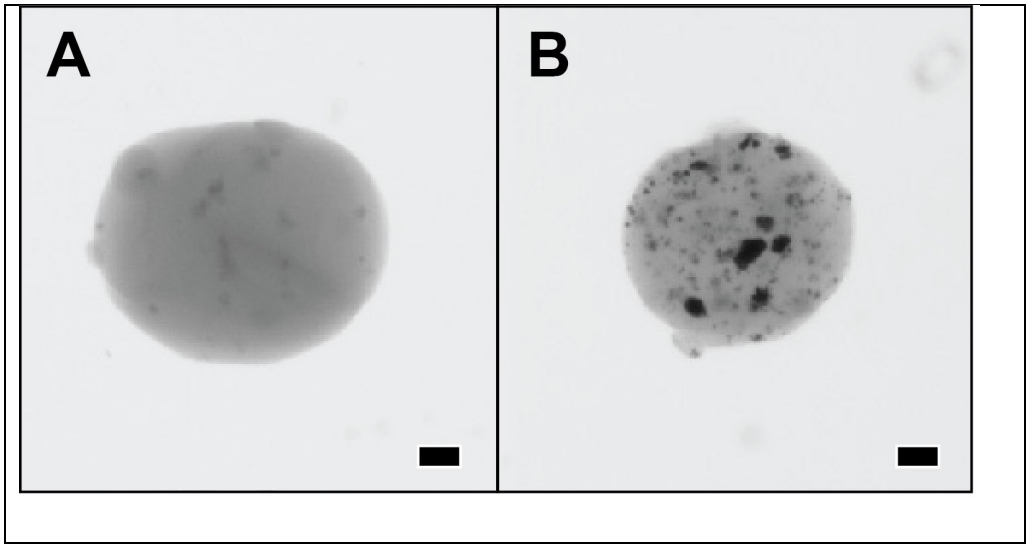

Coatings and paint coupons. In our initial screening experiments, a simple model coating system was used consisting of a waterborne styrene-acrylic latex, $CaCO_3$, and a thickening agent to allow the wet coating material to be poured and coated with ease (10.3 g latex binder, 2.6 g Albafil S10 (70% $CaCO_3$), 0.1 mL Acrysol TT-935 and 9.1 g sterile H_2O). A formula with an acrylic binder was also developed (12.0 g latex, 8.9 g Albafil S10, 0.7 g RM 6000 (DOW) and 2.97 g sterile water). Vegetative cells or spores could be added to the liquid coating before the thickener to enhance mixing. Coatings were made by hand using a single clearance bar applicator (Bird Film Applicator®) with a 4 mil gap or a Leneta WC-1670 Wire-Cator. The wet coating was drawn down on a plastic mat, allowed to dry, and then released from the mat. The free-standing films could be handled without damage and cut into any desired shape.

Scaffold development. Four coatings were made to assess systems where growth media is replaced by a more typical coating formula as a scaffold. These were designed to provide a range of hydrophilicity (simulating the hydrophilic TSA) and a range of porosity, assuming the high porosity would enhance the motility on microbial calcifying activity. All four coatings included $CaCO_3$ as a pigment.

SEM micrographs of cross-sections of the potential scaffolds (Figure 6) confirmed that the samples showed the expected differences in porosity. KRG001 and KRG002 are highly porous. KRG003 and KRG004 are not porous.

Table 2 Design Space for Scaffolds

Sample	Hydrophobicity of latex	Pigment Concentration
KRG001	hydrophilic latex	high
KRG002	hydrophobic latex	high
KRG003	hydrophilic latex	low
KRG004	hydrophobic latex	low

Figure 6. SEM images of cross-sections of the four prospective scaffolds.

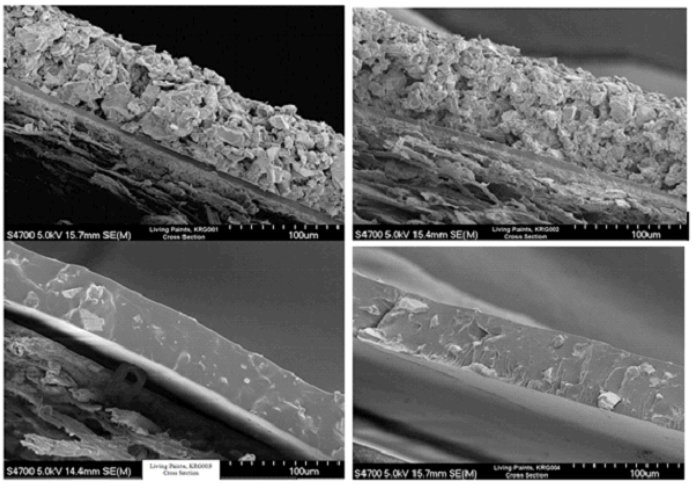

The relative hydrophobicity of the coatings was assessed by drop shape analysis of coatings made in the same way as the SEM samples. Contact angles were measured under ambient conditions using a Kruss Drop Shape Analyzer DSA30S. A 2 µL drop was formed on a 0.5 mm tip and then brought down to touch the surface and deposited. The contact angles are averages of 10 or more droplets of deionized water.

The contact angle results were generally as expected based on the latex chemistry and porosity. Since samples KRG001 and 2 are heterogeneous, water drops initially showed Cassie-Baxter wetting behavior with higher contact angles. After a few seconds, the contact angle decreased as the air in the pores was replaced with water. Samples KRG003 and -004 showed smaller changes or no change in the first 2 seconds. By 20 seconds, all the samples were generally hydrophilic (water contact angle < 90°), ranging from a low of 20° (KRG001), to midrange (65° and 70°, KRG002&3), to a high of 85° (KRG004).

Initial assessment of coating scaffolds, nutrients, and water. Experiments were completed to determine if microbial growth and calcification could be initiated without a growth media scaffold. The coating scaffolds with no added cells/spores were used as a control and demonstrated no growth in any of the conditions. Model coatings with P6A vegetative cells placed on TSA or B4 media scaffolds showed microbial growth and calcification around the edges.

At this early stage, only one of the many variations without growth media showed growth and calcification. Glass slides were coated with KRG001 (hydrophilic binder, high $CaCO_3$) as a scaffold. TSB was added to the scaffold. Vegetative P6A cells were included in the model coating layer. $CaCO_3$ was not included in the model coating layer to more easily distinguish new $CaCO_3$ that might form in proximity to

Table 3. Early conditions that promote microbial growth and calcification.

Scaffold	Coating	Nutrient	Water	Growth
TSA	Styrene acrylic Model Coating	In scaffold	90% RH for 6 days at 30 °C	Y
B4	Styrene acrylic Model Coating	In scaffold	90% RH for 6 days at 30 °C	Y
KRG001	Styrene acrylic Model Coating with no $CaCO_3$	TSB in scaffold	Water applied to surface + 90% RH for 6 days at 30 °C	Y, some calcification

the bacteria. Table 3 summarizes the few conditions that promoted growth and calcification. Figure 7 shows new round features that appear in the hydrated area of a slide where TSB was added to the scaffold and water was applied daily. These features appear in the hydrated portion of the slide and resemble other $CaCO_3$ precipitates seen in liquid culture and on growth media.

Figure 7. Optical micrograph showing new $CaCO_3$ particles within the area that received water (orange arrow). The scale bar is 200 microns.

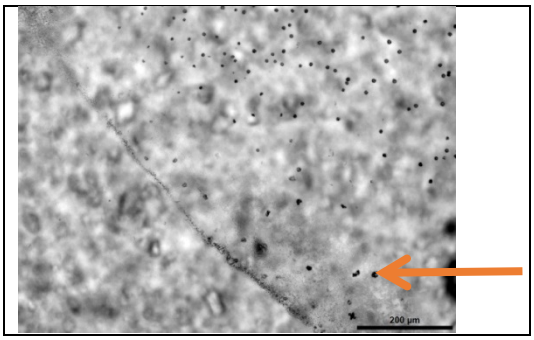

3.1.3 Important Findings and Conclusions

The focus of Task 1 was to identify the materials that would be necessary for a self-healing coating. Non-specific nutrients, organic and inorganic calcium salts, model paint coatings, and coatings-based scaffolds to replace growth media were identified and assessed for suitability. Initial experiments to make a working system showed slight but encouraging success.

Non-specific nutrients were sufficient to prompt growth and calcification. On plates however, minimal media was necessary. Many organic calcium salts were effective in prompting calcification, including calcium propionate which may also be used as in inducer to express genetic modifications (see Tasks 3 and 6). Water is required for the system to work, either as part of an agar scaffold, or manually applied; humidity alone is not sufficient. We were able to provide protection for the microbes, through inducing sporulation or encapsulation.

3.2 Identify functional microbial species (Task 2.1, 2.4, 2.5)

3.2.1 Technical Problems

Functional Microbe. In this task, the goal was to identify a pool of six organisms for the self-healing paint system, in parallel with experiments utilizing P6A, the "proof-of-concept" microbe. In our earlier work, microbes were isolated from calcium-rich environments and identified based on their ability to hyper-secrete $CaCO_3$ in the presence of excess Ca^{2+} ions.[vii] The degree of calcification was the primary capability we assessed. We evaluated additional environmental strains across several bacterial phyla that included both Gram negative and Gram positive species. They were assessed for motility, metabolic flexibility, survival in wet coating formulas, survival in dry paint coupons, and ability to withstand typical paint preservative chemistry.

3.2.2 Technical Results

The primary requirement for the functional microbe is the ability to produce calcium carbonate. Calcification assays were carried out on 88 candidate microbes by growing the strains on B4 media at room temperature for 8 days. Many of the strains proved to be environmental wildtype hyper-secretors. Images of several isolates with notable precipitation were photographed on a Nikon

microscope at 40x magnification (Figure 8). In the figure opaque areas are $CaCO_3$ which can be seen within the area of growth (the darker background) and off the edge of growth. Two polymorphs of $CaCO_3$ were observed in the images, vaterite, which tends to have a rounded habit and calcite, which is faceted.

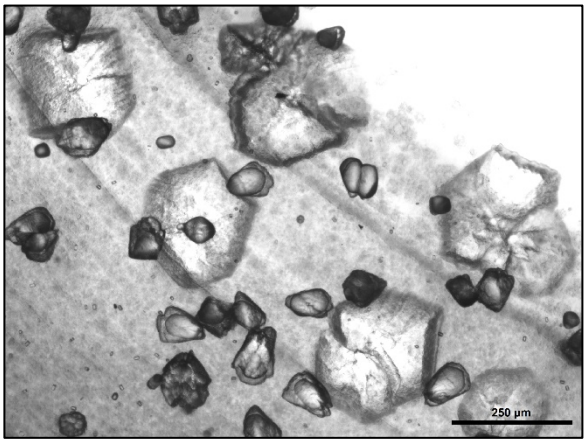

Figure 8. Example calcification assay results. The white area in the top right corner is outside of the streak. Large crystals over 250 µm with angled edges characteristic of the calcite polymorph can be seen close to the boundary of the cell mass. Smaller, more smoothly rounded crystals around 75 µm were observed scattered throughout the cell mass and were hypothesized to be vaterite.

We screened 56 species for swimming, swarming, and twitching motility to determine if any species could be resuscitated at a site distal to the damage and then move toward it. Figure 9 shows the twitching motility assay for a non-motile (left) and motile (right) strain.

Figure 9. Example motility test.

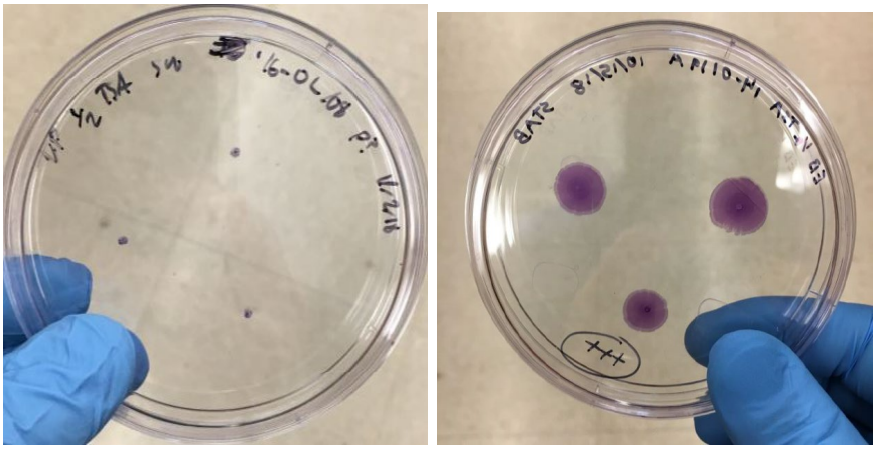

Most commercial coating materials are preserved through the use of biocides. If any of the pool microbes were resistant to typical preservative chemistry, they would represent good candidate species.

The antimicrobial susceptibility of three of our pool strains to four typical in-can preservatives was assessed. Minimum inhibitory concentrations (MIC) were determined at two different pHs for each species. All three organisms evaluated were found to be highly susceptible to the preservatives. Detailed are found below. These results supported our approach of using unpreserved coatings materials. If necessary, tolerant strains could be created through selective mutagenesis.

Table 4 shows the MIC for each of three organisms to 2-benzisothiazolin-3-one (BIT), 2-methyl-4-

Table 4. The MIC of the Proof-of-Concept organism and two pool species with typical coatings preservatives.

Strain ID	Media pH	BIT MIC, (ppm)	MIT MIC, (ppm)	CMIT/MIT MIC, (ppm)	Zpt MIC, (ppm)
P6A	7.3	0.94	7.5	0.43/0.14	7.13
P6A	8.48	3.75	7.5	0.43/0.14	14.25
P12B	7.3	1.88	7.5	0.43/0.14	14.25
P12B	8.48	3.75	1.88	0.43/0.14	14.25
Comamonas 1	7.3	1.88	1.88	0.11/0.04	912
Comamonas 1	8.48	3.75	0.47	0.22/0.07	456

isothiazolin-3-one (MIT), 5-chloro-2methyl-4isothiazolin-3-one (CMIT) in combination with MIT, and zinc pyrithione (Zpt). These results demonstrated that all species were susceptible to typical coating preservatives below typical use levels.

3.2.3 Important Findings and Conclusions

The work of Task 2 was to identify a pool of potential organisms to carry into the Option Phase. Six organisms were identified for this purpose. We were able to down-select to the following organisms: P6A, P12B, *P. aeruginosa* PAO1, *Bacillus megaterium, Comamonas 1*, and additional environmental *Comamonas 2.* This set included a Gram positive, Gram negative, and spore-forming organisms. Initial work with a model *E. coli* system suggested that the pathways to achieve calcification are complicated and can be affected by the available nutrients, pH, and genetics of the microbe.

3.3 Survival in wet and dry coatings (Tasks 2.2, 2.3) and Robustness to Coating Type (Task 4).

3.3.1 Technical Problems

An additional criterion for the functional microbe is the ability to survive in a variety of paints. In early experiments, we explored self-healing systems by making a model coating, introducing the microbes, and coating them immediately. Once the coating was dry (a few hours), experiments could proceed. More effective systems involved long-term survival of the microbes in paint, the ability to remain in suspended animation once dry, and the capability to self-heal when triggered later.

The robustness of the microbes to various coating types was also assessed. We synthesized a variety of binders without preservatives and made model paints to determine the survival of vegetative cells, encapsulated cells and P6A spores over time.

3.3.2 Technical Results

Three latex binders were synthesized without wet-state preservatives (typically included to prevent spoilage) to determine the robustness of our microbial species to various paint chemistries. The chemistries of the binders included a water-based vinyl acrylic (Paint Sample 1/PS1), styrene acrylic (Paint Sample 2/PS2), and acrylic copolymer (Paint Sample 3/PS3). All three binders were formulated into paints containing pigments TiO_2 and $CaCO_3$, thickeners, and typical surfactants and dispersants.

Survival in Coating formulas. To examine the survival of vegetative cells 100 μL of a 3 mL overnight culture in TSB was used to inoculate 3 mL of the various paints. Table 5 shows that all the pool microbes

Table 5. Summary of Vegetative Cell Survival Experiments

Species	Microbial Survival, Vegetative cells (**Y**es, **N**o or **nd** -not done)								
	Paint Sample 1			Paint Sample 2			Paint Sample 3		
	T_0	**48 hr**	**7 days**	**T_0**	**48 hr**	**7 days**	**T_0**	**48 hr**	**7 days**
B. simplex, P6A	Y	N	nd	Y	N	nd	Y	N	nd
B. subtilis, P12B	Y	10^2	N	Y	N	nd	Y	10^2	N
Comamonas 1	Y	N	nd	Y	N	nd	Y	N	nd
B. megaterium	Y	N	nd	Y	N	nd	Y	N	nd
P. aeruginosa	Y	N	nd	Y	N	nd	Y	N	nd

died after a maximum of 7 days in all the paints, regardless of the binder chemistry. All species could be recovered immediately after inoculation into the paint (T_0 in the table). As shown in the table, survival experiments with vegetative cells in the paints were not successful.

To evaluate non-spore formers, the encapsulation procedure developed in Task 1 was used. Larger capsules (~100 microns) were able to protect *Comamonas 1* in the model coating, with survival out to 30 days. Figure 10 shows the Comamonas recovered after 30 days, demonstrating growth and calcification.

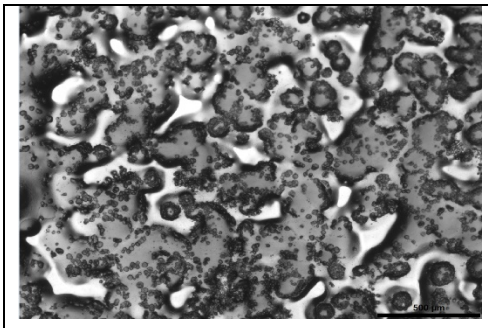

Figure 10. *Comamonas 1* protected by a microcapsule in liquid model paint. The micrograph shows bacteria was that was recovered, demonstrating growth and precipitation.

Survival experiments were also completed in the three paints with spores of P6A. Microbes were viable in liquid vinyl acrylic, styrene-acrylic and acrylic paints at 20 weeks with less than 1 log loss of cells.

Figure 11. Survival of the *Bacillus simplex spores* in Paint Samples 1, 2 and 3.

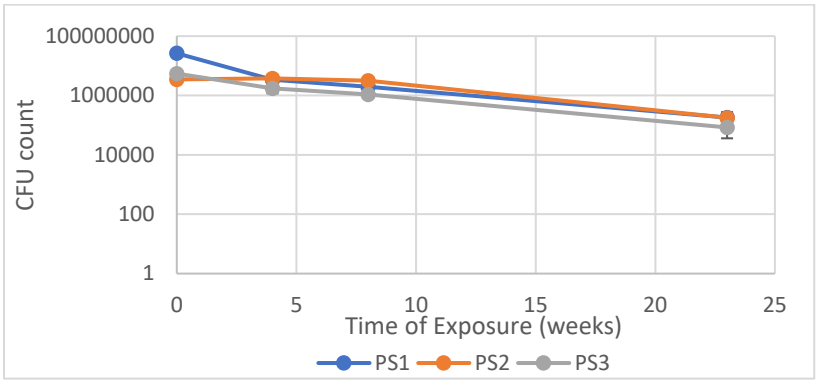

Survival in Model Coating Coupons. Films of the model coating were prepared using 20 mL the model

paint, inoculated and drawn down immediately onto a non-stick polypropylene mat using a Leneta WC-1670 Wire-Cator. The films dried overnight in a laminar flow hood and were cut into 25 mm diameter coupons using a sterile hole punch. Coupons were stored in sterile Petri dishes.

To test for growth and calcification, coupons were plated onto B4 media. Visible growth was observed at 28 days. The photos in Figure 12 demonstrate the ability of spores to be inoculated into a model paint formula at 10^3 cfu/mL, drawn down into a film, dried, and survive for 28 days. This demonstrates that sporulation and subsequent germination do not interfere with the calcification phenotype.

Figure 12. Germination, Growth, and Calcification of Spores in Paint coupons after 28 days

Coupons with 10^3 spores/mL after 28 days at room temperature. Films show no visible growth	**Coupons with 10^3 spores after 28 days at room temperature then incubated at room temperature and humidity for 4 days on B4 media. Films show germination and growth.**
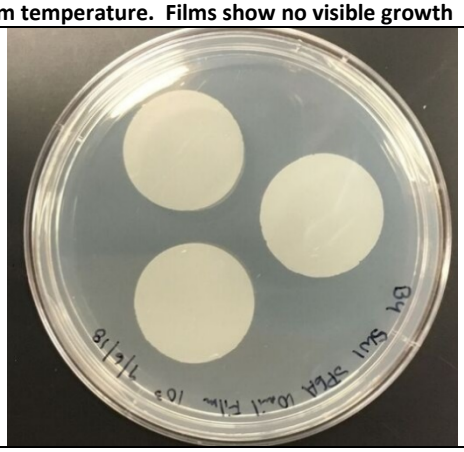	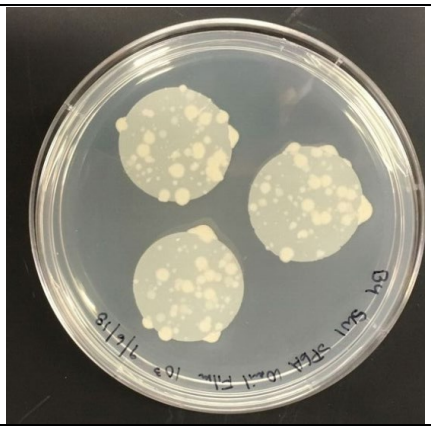

Figure 13. Survival of P6A spores in dry paint coupons

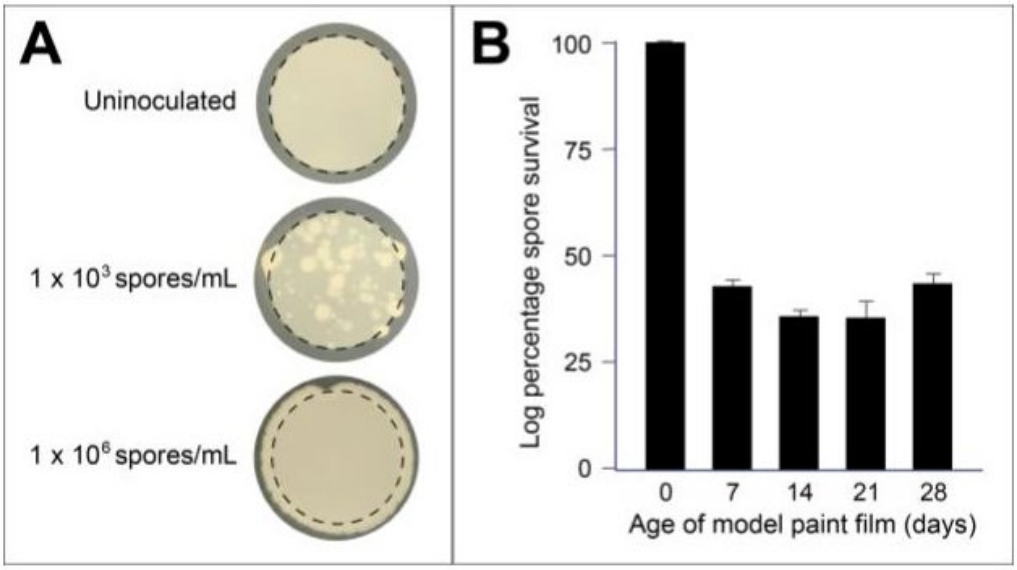

The survival of P6A spores in films of model paint was quantitated. Inoculated films were cut into standard coupon sizes (A) and allowed to grow on B4 support media for 3 days before colonies were counted. Inoculation of ~1 x 10^6 cfu/mL produced confluent growth, so long-term viability was carried out at 3.1 x 10^3 cfu/mL followed by colony counting (Figure 13 A; the dashed line indicates the boundary of the paint coupon). CFUs were calculated as the total cell number in the inoculated volume of the disk (22 mL), and emergent colonies counted by backlighting the film. Survival in dried paint films over 28 days Figure 13 (B) was standardized to percent of survival from growth on day 0.

Visible growth was still observed at 172 days. Figure 14 shows a coupon of model coating that was inoculated with spores, held at room temperature and humidity for over 24 weeks, and then plated to demonstrate growth. The circled region in the image show crack filling as a result of the growth.

Figure 14. Model coating containing P6A spores. After six months of storage in room conditions the P6A was still able to germinate, grow and calcify, and fill cracks (red oval) when it was placed on growth media.

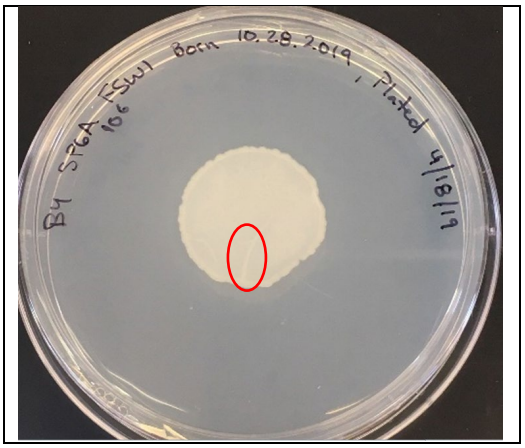

3.3.3 Important Findings and Conclusions

The final critical capability for a self-healing coating is the ability of the microbes to survive in the liquid coating formula, withstand desiccation when the coating is dried, and to subsequently grow and calcify under the desired conditions. In the Base Phase, we were able to demonstrate that P6A spores meet all these criteria. Vegetative cells of the other pool microbes did not survive in the liquid paint, or they were unable to grow and calcify from dried coupons. Alginate microcapsules were capable of protecting one of the Gram negative species for 28 days in a model coating formula. Spores of P6A survived in a dried coupon for >6 months.

3.4 Genetic control and calcification in an *E. coli* model system (Task 3)

3.4.1 Technical Problems

Genetic control. Initial self-healing experiments were conducted with environmental isolates to avoid the complexities of including genetically-modified species within the coatings. However, an effective system requires the microbes to respond very specifically to environmental cues – to grow in response to damage, but not to grow in the wet formulation and dried films until needed. While such functionality may be possible with native phenotypes, we hypothesized that genetic regulatory control would be necessary. Enhancement of calcium transport on the order of 1000x might allow entombment as a mechanism to limit the total production of calcite. Lower levels of enhancement may speed the rate of filling and minimize the amount of microbial growth necessary for filling, reducing reliance on

nutrients or other control mechanisms.

Our first goal was to use an *E. coli* model to determine whether regulatory networks could be modified to enhance calcification and to initiate calcification through the use of an inducible promoter. To do this, we used the calcium succinate B4 media without glucose, which allowed rapid screening of phenotypes.

3.4.2 Technical Results

In Task 3 we identified and cloned genes from *E. coli* into inducible plasmids to allow modification of useful phenotypes. Our initial targets included *chaA*, which controls membrane calcium transport, and the carbonic anhydrase *yadF*, which controls CO_2 fixation and $HCO3^-$ production (Figure 1C). *chaA* and *yadF* were cloned into pPRO24, a plasmid containing a propionate-inducible promoter, P_{Pro}. YadF was shown to be overexpressed, but ChaA was unstable in the DH5α background. The *chaA* and *yadF* genes were also cloned into the pBAD plasmid, which contains an arabinose inducible promoter (P_{BAD}) that displays much tighter regulation until induction. Again, YadF could be over-expressed, but ChaA could not.

Figure 15. YadF expression when induced with Calcium propionate.

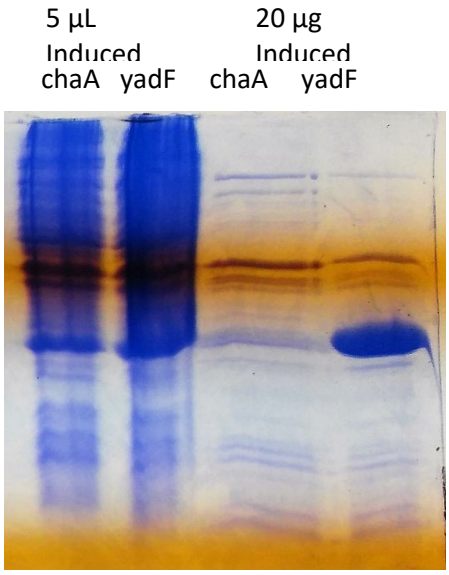

We screened the *E. coli* Keio knockout library to identify additional genetic targets (identified as genes that inhibited calcification). A number of high-potential 'hits' were identified from the knockout library, including *kdpA, mdtH, yrdA, zntB,* and *yohD.* These genes were cloned into the pPRO overexpression plasmid and were assayed for calcification in the presence or absence of the inducer. A difference in calcification was observed only in strains containing the carbonic anhydrase, *yadF,* and the zinc transporter, *zntB*.

To examine the effect of single-copy, stable genomic insertion of these inducible genes on calcification, the gene along with its inducible promoter (P_{Pro}) were inserted into the *E. coli* genome using recombination. The results indicated an increase in calcification with induction, demonstrating that a stable chromosomal insertion still has the desired effect. The presence of the inducer (propionate) had

Figure 16. Induced and uninduced *E. coli.* The figures show three transformed versions of E. coli, each demonstrating that calcification can be increased through induction.

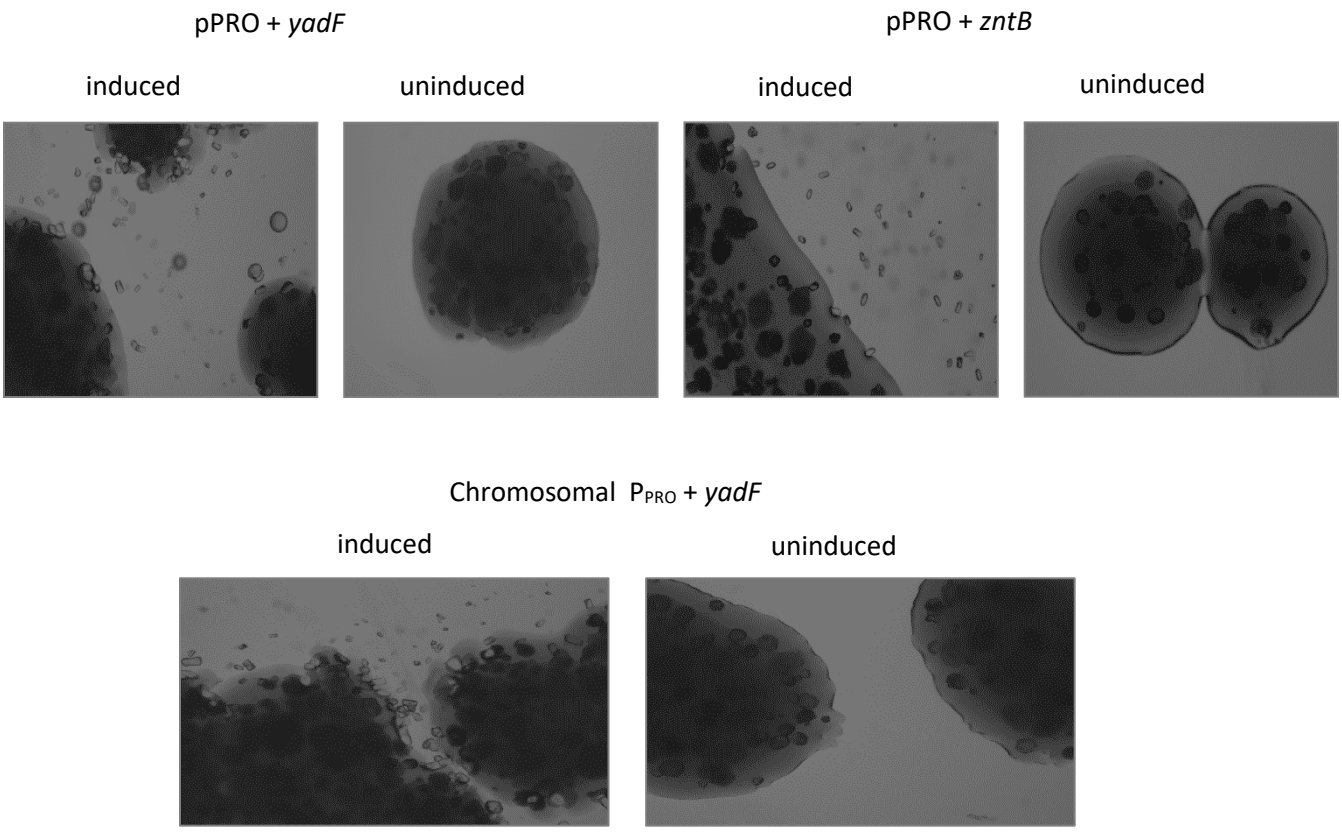

no negative impact on paint formulation, growth, or calcification on solid media. We repeated this construct using a P_{BAD}::*yad*F construct in *E. coli;* however, no difference in calcification was observed when induced.

3.4.3 Important Findings and Conclusions

The native *E. coli* strains used in these assays were incapable of ureolysis, which is the most commonly used pathway for microbial calcification. Our results demonstrated that we identified a viable, alternative approach that has the capacity to be induced by increasing expression of the carbonic anhydrase, *yad*F. Carbonic anhydrases are widely distributed and make an ideal target to overexpress in our functional strains.

Since our method incorporates calcium into the carbon source, the calcium cation is imported into the cell, requiring export to maintain homeostasis. We had hypothesized that increasing the calcium transporter ChaA would increase the rate of calcium export and calcification; however, this was only identified with the zinc transporter, *zntB.* This may be linked to the critical role that ChaA plays in cellular Ca^{2+} homeostasis, decreasing fitness with over-expression of this protein. ZntB may overcome this limitation as a more general divalent cation transporter.

Our results in *E. coli* also demonstrated the critical role that central metabolism and pH have in driving calcification and that a balance between the calcium and carbon sources are critical to the method we invoked.

3.5Genetic control and Calcification in Functional Microbes (Task 6)

3.5.1 Technical Problems

Continuing the genetics work, we sequenced the genomes of several of our target species, including P6A, P12B, and the environmental *Comamonas 1* and *Comamonas 2* to determine whether these species contained the genetic pathways and transcriptional controls that would allow translation of the *E. coli* genetic expression system.

Major technical problems arose from the transformation of the two cave isolate strains *Bacillus simplex* GGC-P6A and *Bacillus subtilis* GGC-P12B. *Bacillus subtilis* are naturally competent. However, competency varies greatly with wild strains. No examples of transformation protocols for *Bacillus simplex* were found in the literature, so our work focused on P12B, with the hope that any results could be transferred to P6A. Five separate approaches to the transformation were attempted. After executing the transformation, we assessed if the enhanced calcification phenotype was demonstrated and if the transformant was stable.

3.5.2 Technical Results

Genetic material from the cave strains P6A and P12B was sent to Arizona State University for whole-genome shotgun sequencing. Sequences were assembled using the program Geneious. The P6A assembly was found to consist of 28 Contigs, 5.6 Mbp total. The P12B assembly consists of 15 contigs, 4.2 Mbp. Genomes were submitted to the Rapid Annotation using Subsystem Technology (RAST) server for annotation. The 16S rRNA gene from P6A had the highest homology to *Bacillus simplex* str NBRC 15720, which is what we previously observed. The 16S gene from P12B had the highest homology to *B. subtilis* str. NCIB 3510.

Annotations of GGC-P6A and GGC-P12B genomes revealed potential targets to overexpress for enhanced calcification. Both strains have a *chaA* homolog, a beta-type carbonic anhydrase (*yadF* homolog), and a gene annotated as an ATP driven calcium pump. No homologs of *zntB* (the *E. coli* transport protein) were identified in either genome.

Annotation of the *Comamonas 1* genome revealed no homologs of *chaA, zntB,* or the Ca-ATPase we found in the two *Bacillus* strains. We identified one carbonic anhydrase gene (*can*), plus six genes that encode cation efflux proteins (including *zip*). No genes were identified as Ca transporters, although zinc transporters (like *zntB*) were identified. Annotation of the *Comamonas 2* genome revealed no homologs of calcium export pumps identified in *E. coli* or the two *Bacillus* strains. Two carbonic anhydrase genes and six gene clusters annotated as cation efflux pumps were identified. Many of these existed in multiple copies.

Transformation of *Comamonas* strains. The *Comamonas 1* and *Comamonas 2* strains were successfully transformed using electroporation. A protocol typically used for *E., coli* was used with slight modifications in the incubation temperature and media used. To prepare competent cells, strains were grown overnight in Super Optimal Broth (SOB). A fresh solution of SOB was inoculated the next day and the cultures were grown to an OD_{600} of 0.6. Cells were then washed four times with 10% glycerol and placed in a -80°C freezer until needed.

The plasmid pBBRMCS-2 (pBBR) was used as an expression strain for both *Comamonas* species. This plasmid contains a derepressed lac operon (binding site for lacR removed). It has been shown to have constitutive expression in a variety of Gram-negative organisms. However, no Comamonas strains were tested (Kovach ME *et al., Gene. 1995*). Fifty ng of plasmid was added to 60 uL aliquots of competent cells, and then electroporated @ 1.8 kV. Cells were recovered in ½ TSB for 2H @ 30°C, then spread onto

½ TSA with an antibiotic (kanamycin) and allowed to incubate overnight. Plasmid was successfully re-isolated from both *Comamonas* strains, indicating both been successfully transformed.

Two genes from *Comamonas 1* were cloned into the plasmid: the native carbonic anhydrase and a zinc exporter (ZIP). One gene from *Comamonas 2* was successfully cloned into the plasmid, annotated as an iron export protein, but with affinity for other divalent cations. An attempt was made to clone the native carbonic anhydrase gene from *Comamonas 2* into pBBR1, but only a truncated fragment was successfully amplified. The plasmids were used to transform either *Comamonas 1* or *Comamonas 2* successfully, and all transformants were confirmed via PCR. Strains remained stable after multiple passages on kanamycin containing plates. Strains were grown in liquid cultures, and total calcium ion content was calculated. Here, the *Comamonas1:: can* strain exhibited slightly higher calcium carbonate production compared to the WT strain (WT generated 296 ppm while the expression strain generated 346 ppm). The calcium concentration from the *Comamonas 1::zip* was identical to the WT strain. Both strains showed a slight increase in the onset time of calcification for the mutants. The *Comamonas* strains were assayed for differences in calcification on agar plates, but there were no observable differences between the engineered strains and the wildtype strains (Figure 18).

Figure 17. Comparison of the level of calcification on solid media. WT Comamonas 1 (left), Comamonas 1::*zip* (right) and Comamonas 1*::can* (lower left).

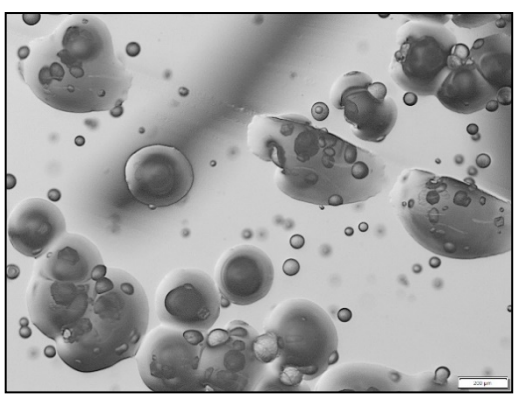

WT. *Comamonas 1*

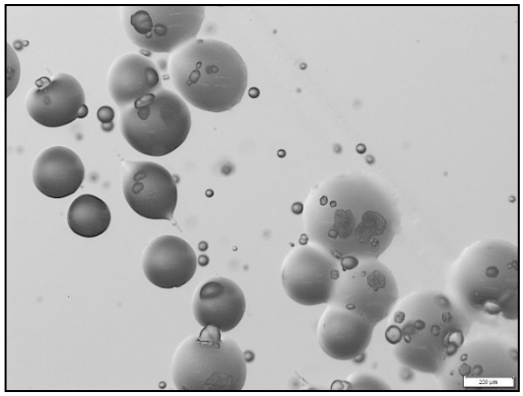

Comamonas 1 + *zip* gene

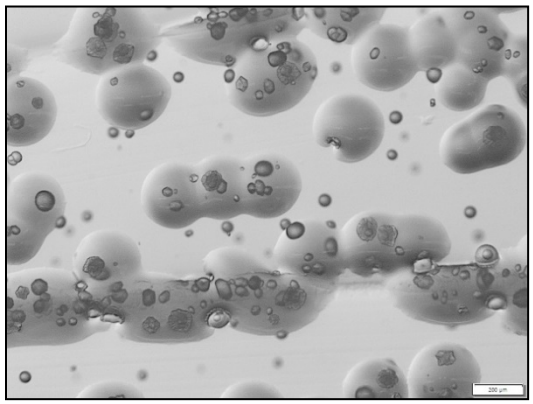

Comamonas 1 + *can* gene

.

Construction of an expression plasmid and transformation of Bacillus strains. The plasmid pDG1730 was initially used to test transformation protocols. This plasmid contains a spectinomycin resistance gene and integrates into the *amyE* locus of *B. subtilis.* Sequencing of the P12B genome revealed an *amyE* gene with 100% sequence identity to the type *B. subtilis* strain using the NCBI genbank database.

Transformation of GGC-P12B. The following protocols were attempted to transform *B. subtilis* str. P12B. One described by Guiziou *et al.* (2016), and an electroporation protocol from the Bacillus Genetic Stock Center (Dr. Dan Zeigler, personal communication, 2019). We also tried protoplast electroporation (Romero *et al.* 2006) and a combination of RbCl and sepiolite (Ren *et al.* 2017). None of these protocols were successful. A PEG/sorbital protocol described by Seo and Schmidt-Dannert (2018) did generate successful transformants, which were confirmed using PCR amplification of the region integrated into the *amyE* locus.

Two genes from GGC-P12B, the native *chaA* gene, and native carbonic anhydrase gene (*can*) were cloned into the pDG1730-Pveg backbone. We transformed P12B with the Pveg-*chaA* plasmid. Calcification between the mutant strains and the WT strain were compared, but we were surprised to see that there was no detectable difference between the two strains.

Figure 18. Comparison of the level of calcification on solid media. WT P12B (right) and the transformed P12B (left).

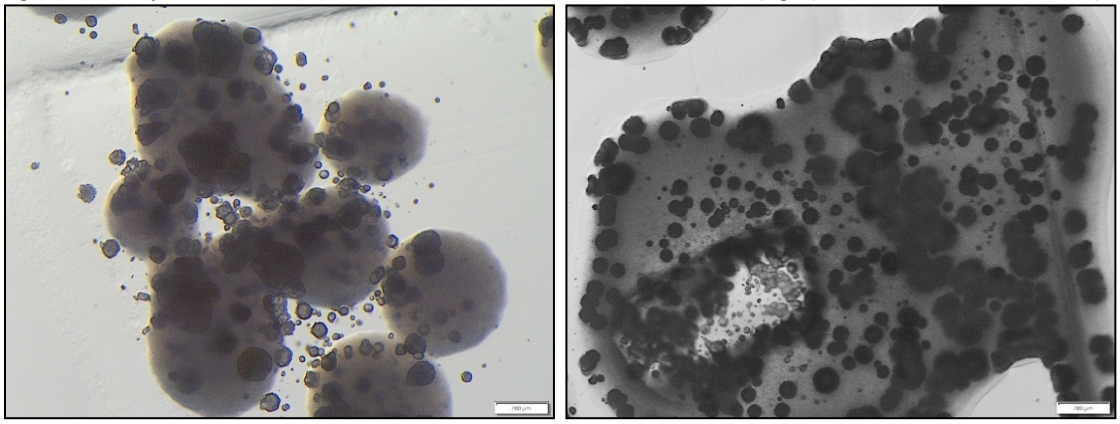

P12B + chaA WT P12B

We did notice that transformants with pDG1730 and its derivatives are unstable, which may be due to dose-dependent toxicity of the expressed genes, or an instability of the insertion cassette (which carried unintended plasmid DNA into the host genome).

3.5.3 Important Findings and Conclusions

Sequencing of the functional strain revealed potential targets that mimic the target genes found to enhance calcification of *E. coli.* A carbonic anhydrase gene, which is a widely distributed enzyme, was found in all the sequenced genomes as predicted. Genes annotated as divalent cation transporters were also identified. Homologs to *ChaA*, the calcium transporter initially identified in *S. typhimurium* as necessary for calcification were identified in both *Bacillus* strains[ix]. Other transport proteins were also identified but were not homologous to ChaA or the ZntB transporter identified in *E. coli.* These results provided numerous targets for overexpression studies.

A workable genetic system was developed for the two strains. The plasmid pBBR1MCS-2, developed as a

broad range Gram negative expression plasmid, could be replicated in both strains. The carbonic anhydrase gene and a zinc transporter protein (ZIP) were introduced into *Comamonas 1.* No impact on calcification was observed on solid media; however, a small increase in calcium carbonate formation was observed in the *can* expression strain in liquid culture.

Although we successfully transformed *E. coli* to demonstrate a calcification phenotype, the same techniques did not enhance the calcification of either Comamonas or P12B.

3.6 Test method development (Tasks 7.1 and 7.2)

3.6.1 Technical Problems

An x-ray powder diffraction (XRD) approach was needed to determine the crystal structure of polymorphs for representative and leading samples of $CaCO_3$. Quantitative photographic image analysis methods were needed to determine the extent of calcification in solid media and at the site of repair in damaged coupons. Experiments have suggested[x] that local pH and ion chemistry can be used to influence polymorph formation and hence the type of healing induced. A method to concurrently measure $CaCO_3$ production, pH, and microbial growth rate in liquid media was needed as well.

3.6.2 Technical Results

Polymorphs of calcium carbonate have been successfully and reliably detected with XRD analysis in prepared cultures grown for one week at room temperature with shaking at 100 rpm on an SKC-6200 orbital platform shaker. The precipitated minerals were collected by vacuum filtration of the culture onto an MF-Millipore 8.0 µm MCE membrane and washed of cell debris with 15 mL of a 20mM HEPES buffer at pH 8.3. These filters were allowed to dry for 1 hour at room temperature, scraped into a 10 mL glass tube, and allowed to dry for an additional 24 hours before XRD analysis with an Ultima IV X-ray diffractometer. Identification of the diffraction profiles was determined using the PDXL 2.1 software package (Rigaku). Using this method, vaterite and calcite were identified individually and in combination produced from *E. coli* K12, P6A, P12B, and *Comamonas 1*.

An image analysis method to quantify the calcification in solid media was developed using an Olympus SZX7 microscope equipped with an Olympus SC180 camera. Images were captured using cellSens Standard 2 software (Olympus) and analyzed using the ImageJ plugins Trainable Weka Segmentation (TWS; v3.2.33) and MorphoLibJ (v1.4.1) to measure calcification[xi,xii]. The TWS plugin image feature recognition algorithm was used to identify carbonate crystals on the colony using a set of training images of colonies from the same plate, followed by manually designating areas as crystal (red), colony (green), or background (purple) to generate an overlay output. The classification was then scored as a .model file for use with other images of similar morphology, which was further refined with additional training images of a series. The plugin analyzed subsequent images using this training set and calculated a probability map showing coverage of colonies by calcite crystals. Once crystals were identified and segmented, percent coverage was calculated using the Analyze Particles function built into ImageJ.

Particle analysis was used to obtain individual crystal information. The ImageJ TWS Get probability function was used to generate a probability map of each colony. The image was then formatted as an 8-bit image. The threshold values were adjusted until the calcite crystals were selected, and the “analyze particles” function was used. The minimum size of pixel units was used to mitigate artifact errors. A TWS analysis to give an ROI overlay allowed measurements of the area selections to be saved as .csv files. For the best results, multiple classifiers were produced to account for the change in colony thickness and shadow gradient effects as the colonies grew, changed shape, and became increasingly opaque and

occupied by crystals over time. The final overlay of crystal coverage generated by the particle analysis was periodically applied back to the original colony image to check the accuracy of the fit of the classifier and adjusted where necessary.

Figure 19. Training set for image analysis showing the initial image, A, partial identification of crystal (red) and colony area (green), B, and full indentification, C.

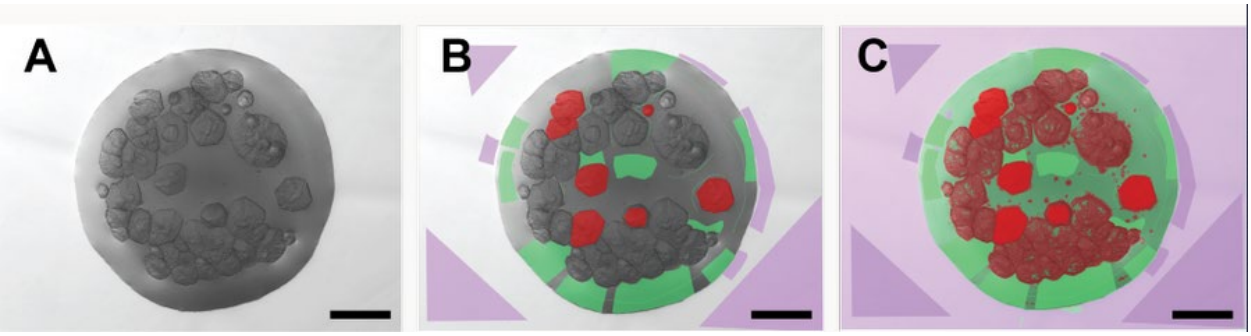

A method for quantification of calcification in liquid media was also developed. Cultures were grown with shaking (250 rpm) on an Excella E24 incubated shaker and growth was recorded. Once the optical density reached OD600 0.1, 1 mL samples were taken every hour to quantify $CaCO_3$ precipitation. To do this, 1 mL samples were filtered onto a 25 mm Isopore 0.2 µm black PC membrane using a micro-syringe 25 mm filter holder and then washed 10 mL 20 mM HEPES buffer (adjusted to pH 8.3). The membrane was then submerged in 10 mL of a 5% nitric acid for 30 minutes to dissolve any calcite and centrifuged to remove any cell debris. The calcium concentrations of the resulting HNO_3 acid solution was measured using a 700 Series ICP-OES. Wavelength calibrations were completed using a 5 ppm Mn calibration solution, with standards prepared from a 10 ppm calcium stock solution. Analysis of calcium concentration (per mL of culture) was then carried out using ICP Expert II software

Figure 20. Method to monitor growth, pH and calcium concentration in liquid media. Calcium concentration (ppm) and optical density during the experiment are on the primary axis, pH changes during this period are on the secondary axis. The calcium salt for each experiment is noted in the lower right.

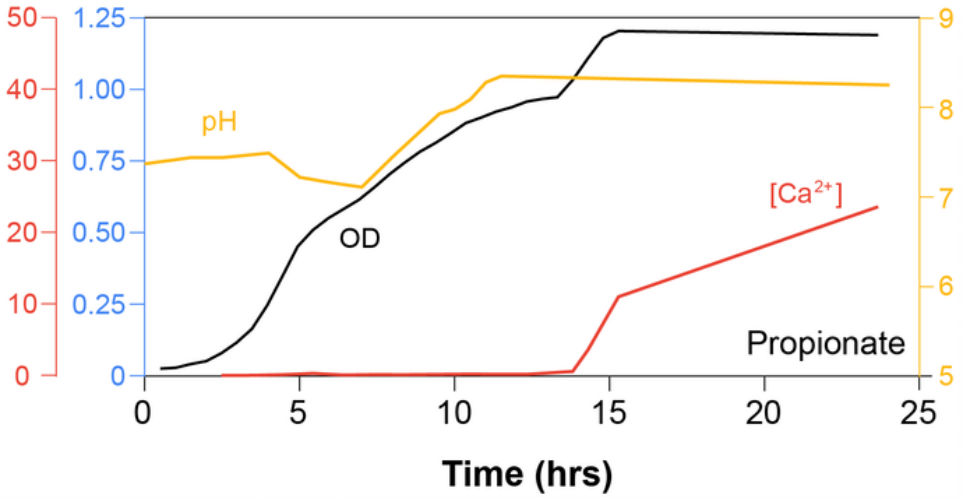

3.6.3 Important Findings and Conclusions

The development of these methods allowed us to examine calcification under a number of metabolic conditions that were not previously possible. This included examining the influence of humidity on crystal growth and the relationship between metabolism on calcification and polymorph structure.

3.7 Optimize control of microbial growth (Tasks 5.1- 5.7)

3.7.1 Technical Problems

After the intrinsic or engineered capabilities of the self-healing system were developed, they were integrated into our functional paint system, and the resulting systems were assessed for self-healing. Determination of the impact of nutrient load and chemistry was undertaken to establish the profile and levels for controllable growth. We varied the type of nutrient looking at the role of amino acids and more specific carbon sources such as organic calcium salts.

To optimize control of microbial growth and precipitation, the impact of the calcium ion source and delivery systems on calcite precipitation was assessed. To demonstrate the potential to precipitate a variety of minerals, including ones that might enhance opacity or durability, we evaluated the effect of the calcium ion source in combination with other metal cations in a model *E. coli* system.

Our early success was with vegetative bacterial cells added directly to the coating formulation. Based on results in Task 2, spores, which might provide a route to longer survival in liquid and dried paints, were also assessed in Task 5.

Our early self-healing structures were based on nutrients added in an agar scaffold, and assessment of the nutrient load and type continued to be in solid or liquid media. A more effective system was expected to incorporate nutrients directly into the coating. Nutrient delivery as a topical solution was also investigated to enhance control over the growth of organisms in undamaged locations.

Given the 1:1:1 molar ratio of the Ca^{2+}:CO_2:H_2O involved in calcification, approaches to provide excess Ca^{2+} within the self-healing system was of interest, so that local depletion would not lead to the mass movement/thinning phenomenon observed in other self-healing systems. We initiated the proof-of-concept work with a particulate approach. In this Task we also assessed the impact of organic calcium salts, first in liquid media for a model system, then on solid media for the pool microbes.

In early experiments, the water for activation was delivered as part of the agar scaffold. This system worked well for assay development, but an agar scaffold is not practical for use in the field. An effective system needs an alternative mechanism to deliver water to the coating. In this task we evaluated the approach of adding water directly to the coating surface, as well as determining if humidity could be used to trigger growth and calcification.

3.7.2 Technical Results

Nutrient Type. Several microbial strains were incubated in TSB containing one of four amino acids: arginine, histidine, lysine, and tryptophan, to determine if the use of amide-containing amino acids affected culture pH and rate of calcification. The three environmental strains, *Bacillus simplex* (P6A), *Bacillus subtilis* (P12B), and *Comamonas 1* were incubated for 48 h at room temperature. All the amino acids produced solutions that were above a pH of 8.3, which promote calcification. Although there was some variation, TSB was one of the best nutrient sources for each of the strains.

Calcium Ion Source. ICP-OES was used to analyze the bacterial strain throughout its growth phase and link it to pH changes in the culture. This approach is demonstrated Figure 21, where *E. coli* K12 was

grown using different calcium salts. The results indicated a jump in optical density which coincides with an increase in pH (generally >8.3) and the onset of calcification. This served as a proxy for the onset of calcification in liquid media and was used as a rapid screen for such microbial activity in various solutions. Using this approach, there were notable differences between calcium sources in terms of growth time, the time point of calcification, and total calcification (measured in Ca^{2+} μg/mL). This indicated that when *E. coli* was grown on media that do not promote the full TCA cycle, calcification was increased, likely due to the necessity for CO_2 utilization and an increase in culture pH (from the removal of carbonic acid).

Figure 21. E.coli growth over 24 hours at 37 C with calcium concentrations (ppm) and optical density. pH changes during this period are on the secondary axis. The calcium salt for each experiment is noted in the lower right.

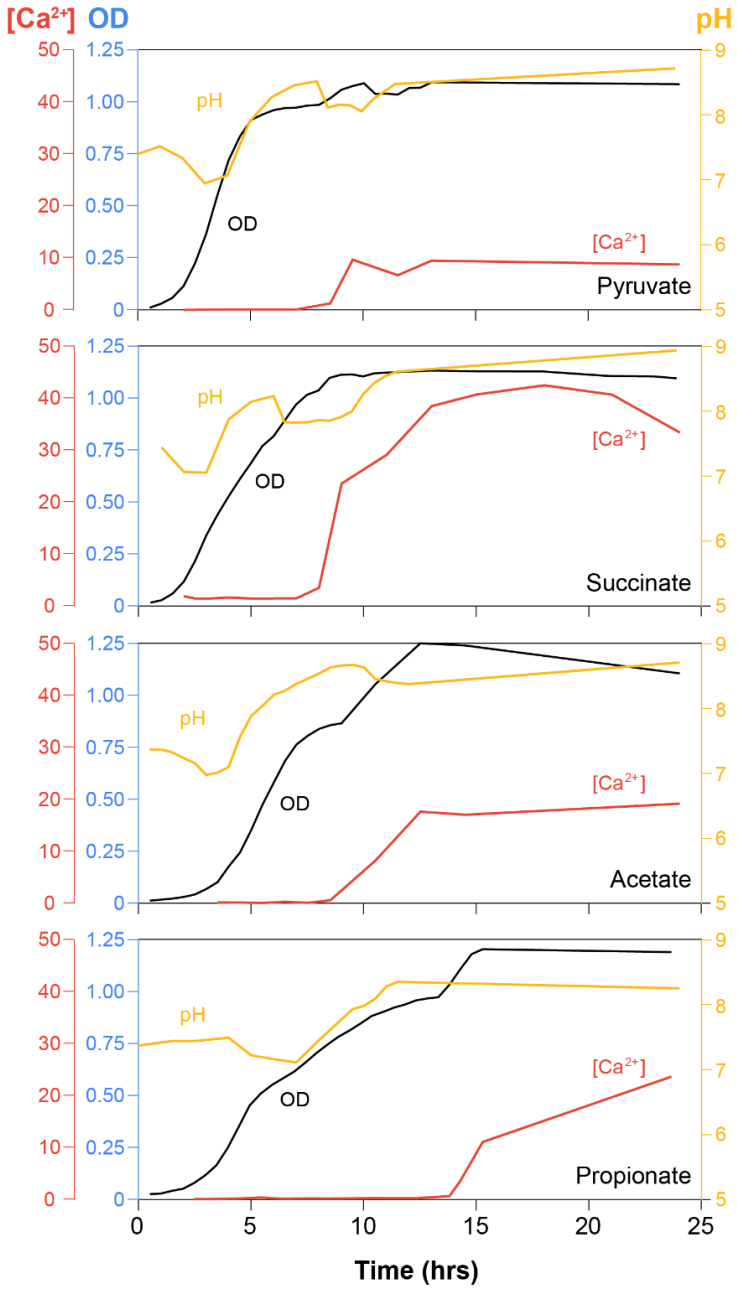

On solid media, the six pool microbes identified in Task 2 were grown to examine the impact of various calcium salts on calcification in a process that would most mimic their activity in coatings. Again, calcium succinate promoted calcification, along with calcium citrate (which could not be utilized in *E. coli). P. aeruginosa* PA01 was the most robust to calcium source, with some amount of calcification in all the organic salts. Calcium succinate and citrate were the most likely organic calcium sources to enhance calcification across all calcium sources.

Table 6. Calcification by Functional Strains on various Calcium Sources

	Calcium source				
Strain	**Propionate**	**Pyruvate**	**Lactate**	**Succinate**	**Citrate**
Environmental Comamonas 1	No growth	Slight calcification	Good calcification, spreading colonies	Good calcification, extends away from the colony	*Best calcification, extends away from the colony
Environmental Comamonas 2	Good calcification	Good calcification	Poor growth and calcification	*Best calcification, extends away from the colony	No calcification
B. megaterium	No calcification	Slight calcification	Poor growth and calcification	*Best calcification, extends away from the colony	Good calcification, extends away from the colony
B. simplex P6A	Slight calcification	Slight calcification	Slight calcification	Slight calcification	*Best calcification
B. subtilis P12B	No calcification	Slight calcification	Poor growth and calcification	*Best calcification, extends away from colony	Good calcification, extends away from colony
P. aeruginosa PA01	Good calcification	Good calcification	Good calcification	*Good calcification, extends away from the colony	*Best calcification, extends away from the colony

The effect of the calcium ion source on enhanced opacity or durability was assessed by a series of experiments in liquid media with a model species: *E. coli* K12. Depending on the ratio and source of calcium and magnesium, *E. coli* was able to produce magnesium-rich calcite, monohydrocalcite, or aragonite. The magnesium-rich calcite in combination with the monohydrocalcite (Mg/C molar ratio <6; $MgSO_4$ as the Mg source) appeared whiter and brighter than either the magnesium-rich calcite alone or the aragonite.

Expansion of this work to produce dolomite, which is harder than the calcites, and more likely to be resistant to weathering was also successful in liquid media. A series of dolomitic minerals were precipitated by E. coli by the addition of manganese and other ions. The dolomitic minerals included ankerite ($Ca(Fe, Mg, Mn)(CO_3)_2$), kutnohorite ($CaMn^{2+}(CO_3)_2$), rhodochrosite ($MnCO_3$), and dolomite ($CaMg(CO_3)_2$). These minerals were observed co-precipitating with each other in various configurations depending on the concentration of magnesium, manganese, and sulfate ions in culture. Distinct crystal morphologies for the precipitated minerals were observed with scanning electron microscopy and were found to have different diffraction patterns by XRD.

Figure 22. Diffraction profiles and SEM micrographs showing co-precipitation of ankerite with A. kutnohorite (1500x mag) and B. dolomite (4000x) from *E. coli* liquid cultures

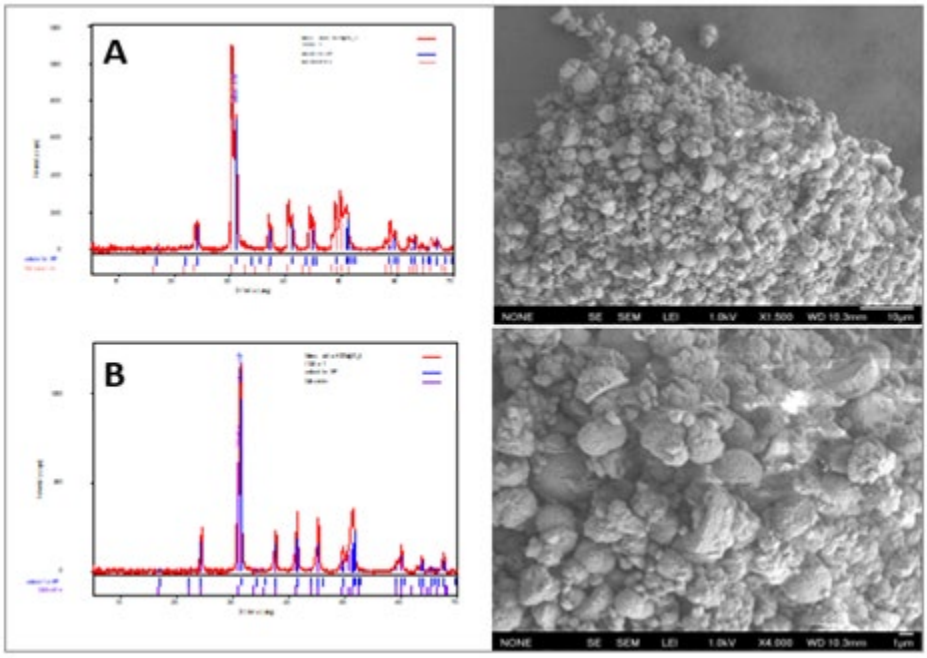

Experiments to control the polymorph precipitation through the ratio of calcium and magnesium ions were translated from the model *E. coli* system to *Comamonas 1*. Aragonite precipitation was induced in liquid culture. (Previous experiments in *Comamonas 1* only produced calcite and vaterite).

Water delivery. Since water is essential, most of the practical experiments were carried out in high humidity to enhance the likelihood of growth. However, we assessed the impact of $CaCO_3$ crystal growth in varying humidity environments. Calcium succinate agar plates were inoculated with dilutions of *E. coli* K12 (10^7 and 10^8) and left to grow in environments of different relative humidity. Plates were initially incubated at 37°C for 24 hours to allow colonies to establish. After this, the plates were transferred to one of three treatments: a) ~0% relative humidity (RH), a sealed plastic container with a desiccant inside, b) benchtop at ambient room temperature and humidity, c) 70% RH inside an environmental chamber.

The plates were imaged at the same time of day at 24 hrs, 48 hrs, and 72 hrs after inoculation. ImageJ and Trainable Weka Segmentation were used to process and segment the images according to the area occupied by colony or crystals. A percentage area of $CaCO_3$ crystals was calculated and used as the basis

for the comparison between treatments. Colonies were selected based on their position relative to other colonies on the plate. Ideal colonies were isolated such that they could be singularly imaged in a frame, but still maintain proximity to other colonies that were representative of the plate dilution, to retain the effects of colony density on calcification. Dilutions of 10^{7} and 10^{8} fulfilled these criteria best. Lower dilutions than this resulted in plates that were too colony dense and unsuitable for single colony analysis.

Increasing the humidity of the immediate environment to which the bacterial colonies were exposed appeared to result in larger crystals and overall higher crystal coverage (Figure 23). The highest percentage of colony area occupied by crystals between treatments was observed on the plates that were kept at 70% RH (30.3% coverage). The least percentage calcification cover was observed on the plates kept at 0% RH, suggesting humidity may play an important role in crystal size, formation and strength of the repair in coatings.

Figure 23. Comparison of single bacterial colony calcification grown in different humidity environments (0: 0% RH, A: 50% RH, 7: 70% RH). Individual colonies of *E. coli* representative of the whole plate, grown on succinate minimal agar at 10^{7} dilution, were imaged at 24, 48 and 72 hours. Scale bar represents 500 µm. Contrast-enhanced and background removed to increase the visibility of crystals inside the colonies.

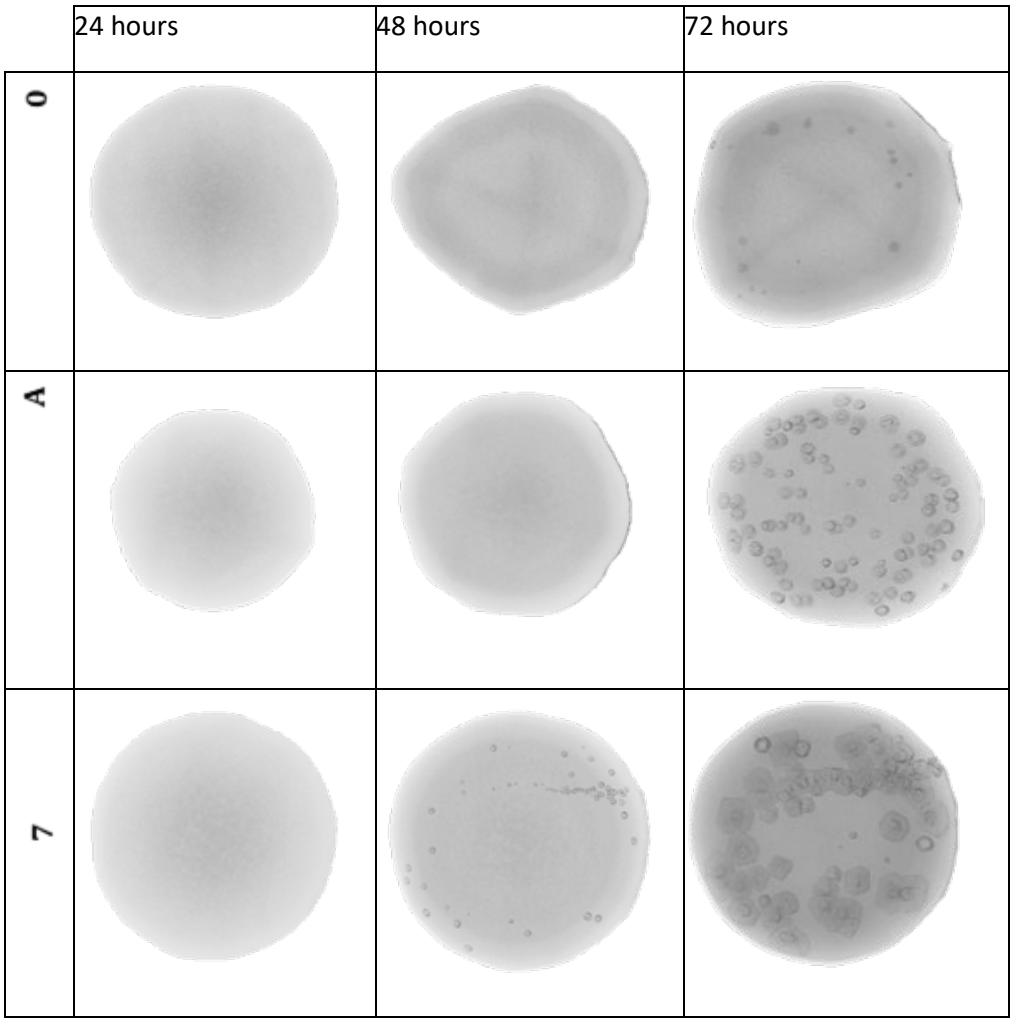

Figure 24. Relationship between the size of calcium carbonate crystals, the duration of growth, and the relative humidity for *E. coli* grown on succinate agar.

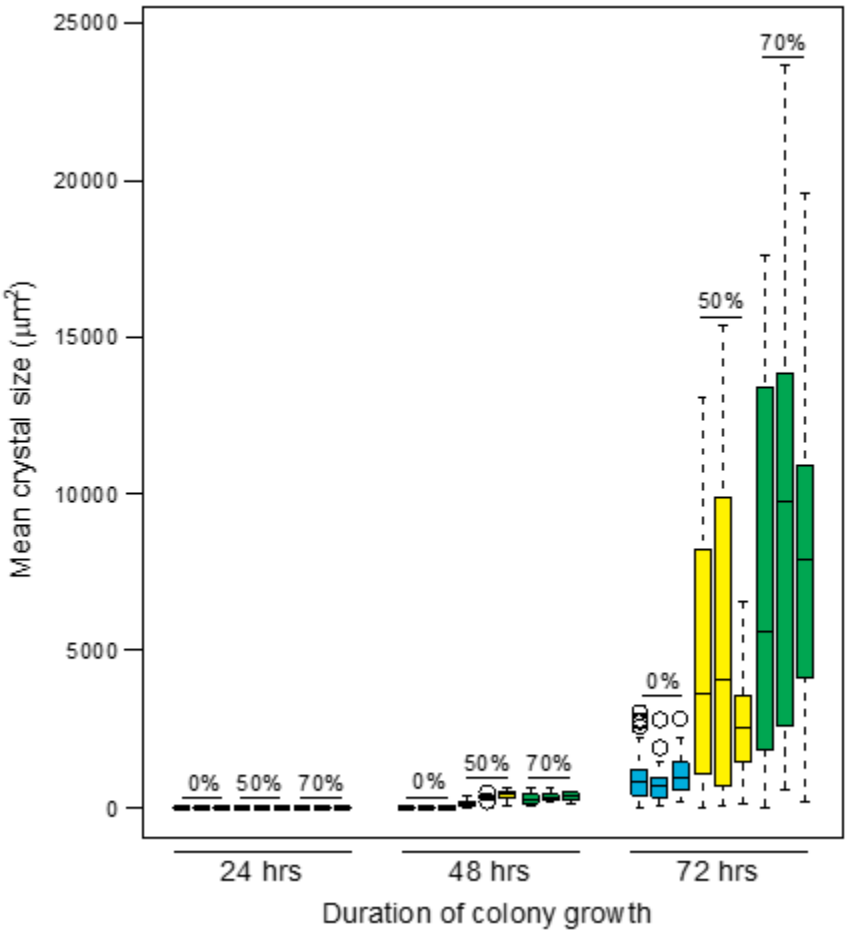

The timing of calcification was also affected by relative humidity. In this experiment, colonies treated with 70% RH calcified sooner than the other two humidity treatments, with crystals evident as soon as 48 hours after inoculation. In contrast, desiccated colonies kept at 0% RH didn't show calcification until 72 hours.

Best Case Delivery System. This experiment followed on the work in Task 1 that suggested that $CaCO_3$ incorporated as part of our model coating could be used to provide the calcium. Coatings were prepared with a range of concentrations of P6A spores and then applied to glass slides. To enhance the likelihood of growth and calcification, the slides were stored in a humidified chamber. Each day the coatings were wet with TSB.

The coatings showed microbial growth and calcification only where the TSB was applied, which highlighted the importance of water and a carbon source to initiate microbial growth. The amount of growth and calcification was proportional to the spore loading. Experiments in which calcium citrate

Table 7. Best Case parameters

Scaffold	None, model coatings applied to glass slides
Nutrient Type	TSB, two levels. Calcium citrate minimal media
Calcium Type.	0.7 micron $CaCO_3$
Microbe Type	P6A spores at $10^{3, 4, 5, 6}$ /ml
Microbe delivery	In coating
Nutrient delivery	Manually spotted on coating daily for 5 days
Calcium delivery	In coating
Water delivery	Humidified, with TSB applied to the coating

minimal media was used instead of TSB also demonstrated growth and calcification, but they did not show any obvious advantages.

Figure 25 shows a 4x micrograph of a model paint containing 10^6 spores/40 mL and applied to a glass slide. After one day in a high humidity environment with TSB spotted on the coating, a white crystalline haze was visible by eye. The large crystals in the picture (about 10-20 microns) were much larger than the 0.7 micron $CaCO_3$ added to the coating. Since the rate at which the new crystals form is correlated with the number of spores added, the mechanism is most likely microbially-mediated calcification.

Figure 25. Micrograph of microbial growth and calcium carbonate crystals produced on model coatings with P6A spores. The amount of $CaCO_3$ was correlated to the number of spores added. Samples with no TSB added to the surface showed no growth or calcification, even though they were exposed to high humidity.

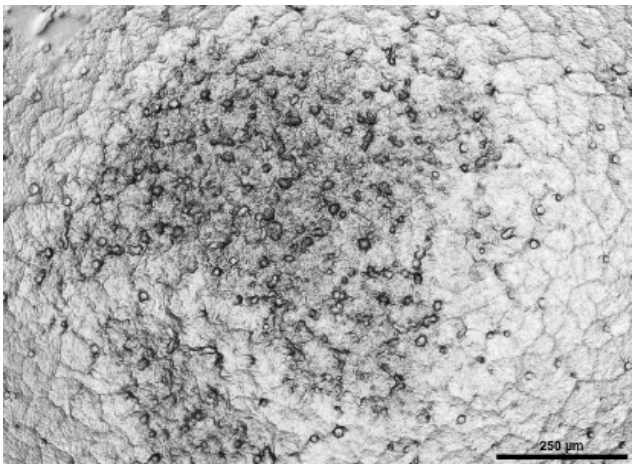

3.7.3 Important Findings and Conclusions

Water was generally a trigger for calcification, either from an agar scaffold (Figure 12), or from TSB or water applied directly to coating coupons, (Figure 25). If an agar scaffold was used, humidity played a strong role in the rate of calcification, with virtually no calcification at 72 hours at 0% RH, whereas plates at 50% and 70% RH show strong calcification at 72 hours. For systems where water or TSB was manually applied, the pH of the water was preferably over 8 in order to prevent the dissolution of $CaCO_3$.

The optimal conditions for growth included TSB as the nutrient. No individual amino acids reliably

enhanced growth beyond the level achieved with TSB. We observed that organic calcium salts had different levels of calcification with each microbe, however calcium succinate or calcium citrate promoted calcification in several species. Calcium carbonate itself was able to provide calcium ions and promote calcification as well. This is advantageous because it is typically included in coating formulations. The addition of magnesium, iron and manganese allowed *E. coli* to produce a variety of minerals.

3.8 Scaffold approaches to replace growth media (Tasks 5.5, 5.7, and 5.8).

3.8.1 Technical Problems

In the proof-of-concept work preceding this project, an agar scaffold provided a source of moisture (which was incorporated in the gel structure), a way for the microbes to move to the site of damage, and the opportunity for spatial segregation of nutrients. However, an agar scaffold is not a practical solution use outside of a laboratory experiment. In this Task we assessed various structures to replace the agar scaffold. Approaches with no scaffold were attempted, but the advantage of a two-layer system to provide a way to segregate nutrients and promoters makes it a more desirable approach.

3.8.2 Technical Results

A variety of primers, topcoats, and microbial delivery approaches were assessed to make a system without growth media. The general structures investigated are depicted below (Figure 26), with scaffold layers made of model paint (with or without 6% TSB) coated on a glass slide, and then recoated with a top coat of model paint that contains P6A. Both P6A spores and vegetative cells were investigated since they have both shown the ability to grow and germinate in coupons of the two model coatings when plated directly on growth media. The six different model paints described in Section 3.1.2 were investigated as scaffolds, and the two model coatings were investigated as topcoats. All the scaffolds and topcoats contained calcium carbonate, which was the sole source of calcium in the system. The first layer (scaffold) was applied to a glass slide at 2 mil wet coverage. The topcoat of inoculated paint was applied at 4 mil. The paint films were scored with a knife in two places to simulate damage to the coating, each cut producing a gap of approx. 1-2 mm.

Figure 26. Structure of coating system without growth media.

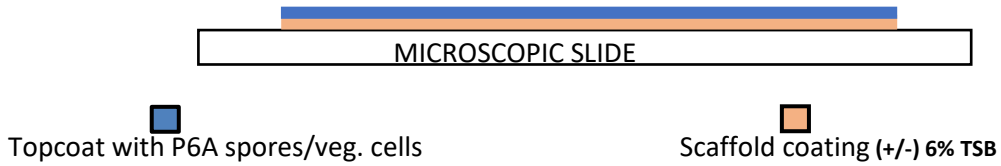

To prompt growth without dissolving $CaCO_3$, 50 µL sterilized H_2O at pH 8 was applied on top of one cut each day. The other cut was left dry as a control. Four slides of each scaffold/topcoat combination were made. Two were placed in a humidity chamber at 70% RH and 25°C, while another set of two were kept at room conditions. Only samples that were at 70% RH showed any growth or precipitation.

Table 8 summarizes results from these growth experiments. Pictures of the samples with successful growth and calcification are below; however, the amount of growth was substantially short of our program goal for growth rate (2.5 mm^3 in 1 week).

Table 8. Conditions and Results for Scaffold/Topcoat Experiments

Scaffold / Topcoat	Results
A. KRG001 + 6% TSB / styrene acrylic coating + P6A spores	Possible growth in humidified condition
B. KRG002 + 6% TSB / styrene acrylic coating + P6A spores	No growth
C. KRG003 + 6% TSB / styrene acrylic coating + P6A spores	Growth and precipitation
D. KRG004 + 6% TSB / styrene acrylic coating + P6A spores	Possible growth in humidified condition
E. KRG003 + 6% TSB / styrene acrylic coating + P6A vegetative cells	Growth and precipitation
F. KRG003 / styrene acrylic coating+ P6A spores	TSB application, growth and precipitation
G. KRG003 + 6% TSB / styrene acrylic coating + P6A veg. cells	Control. No water, no growth
H. KRG003 / styrene acrylic coating	Control. TSB or water application, no growth

Figure 27. Control and Test slides with scaffold and topcoats. The control slide (H) has no TSB or microbes in the scaffold or the topcoat. The Test slide (C) has TSB in the scaffold and P6A spores in the topcoat. The damage reveals the scaffold below (red arrows). Water was applied to the top of both coatings over the damaged area. The control slide shows some calcification at the edge of the crack (black arrow), presumably from the dissolution and re-precipitation. The test coating shows more extensive calcification that can be seen on the edge of the crack (yellow box).

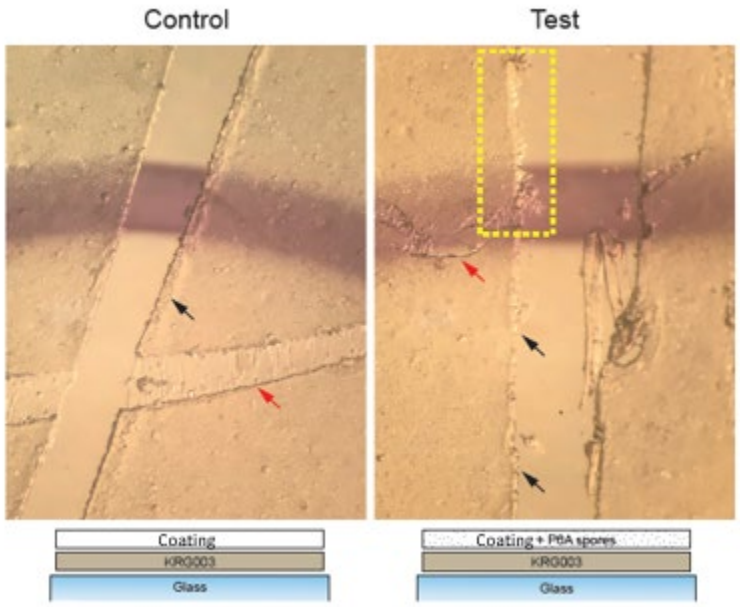

Figure 28. Coating G contained TSB in the KRG003 scaffold and P6A vegetative cells in the styrene-acrylic topcoat. The coating was damaged in several areas and some of them received "Water" on the top, others received "No Water." Calcite crystals (possible vaterite; black arrows) are only seen where the water was added. The white boxes show areas of obvious microbial growth. The yellow box indicates an area where the microbial growth appears to have spread into the crack, with precipitation.

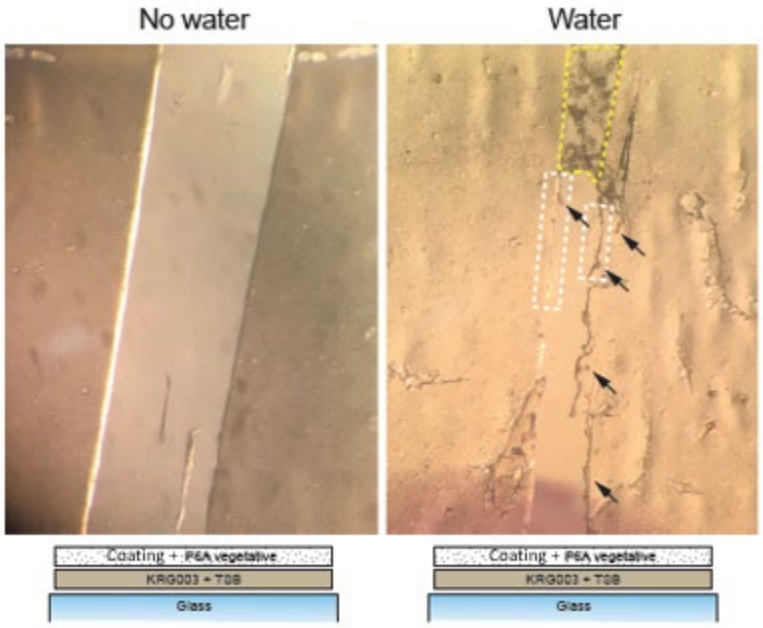

3.8.3 Important Findings and Conclusions

Replacing the growth media was the most challenging element of the project. In our base case system, the growth media provides hydration and nutrients, and the spatial separation of the media and the coupon gives an element of control to the self-healing process. (Until the coupon is in contact with the media, there is no growth or calcification at room conditions). Nutrients and calcium sources that are poorly compatible with coating formulations may be accessed by incorporating them into the growth media. Although the amount of growth and calcification that was achieved with the coatings material scaffolds was small, it demonstrated that it is possible to create a system with no growth media, as long as alternative approaches for incorporating moisture, nutrients and the calcium source are addressed. In our system the manual application of water, incorporation of TSB (nutrients) in the scaffold, and calcium sourced from the coating itself was a successful combination to promote growth and calcification in the damaged areas.

3.9 System characterization (Tasks 7.3 & 7.4)

3.9.1 Technical Problems

After damaged samples were healed, approaches to assess the coating performance were needed. To this end we tested several samples that appeared to be wholly filled (by visual inspection) for film cohesion and compared results to undamaged coatings and coatings that were mechanically healed by repainting. Another approach to assess the durability of the coatings that was evaluated was a standard coatings test for Washability (ASTM D4828-94). This test requires wetting the samples and would allow a

determination if this would trigger unwanted microbial growth.

3.9.2 Technical Results

Model coatings were made with styrene-acrylic and acrylic binders described in Task 1. Each paint was divided into three samples: a control sample and samples containing either 10^6 P6A spores or 10^6 P6A vegetative cells.

Two unpreserved paints (PS3 and PS2) were also divided into control samples and samples containing either 10^6 P6A spores or 10^6 P6A vegetative cells. The paints were coated using a square (90 mm x 90 mm) BYK stainless steel applicator 10 mil edge onto a plastic mat and allowed to dry for an hour. The coatings were detached from the plastic mat, trimmed into rectangular coupons about 2 cm x 8 cm, and for each type of sample, were treated in the following ways, described in Table 9.

Table 9. The following 11 samples were made from each of the four coatings:

Sample	Cell type	Treatment
1	none	Control
2	none	Incubate
3	none	Damage and repaint
4	Spore	Control
5	Spore	Incubate
6	Spore	Damage and repaint
7	Spore	Damage and regrow
8	Vegetative	Control
9	Vegetative	Incubate
10	Vegetative	Damage and repaint
11	Vegetative	Damage and regrow

The treatments referenced in the table were:

- Control treatment: the coupon was stored in a clean, dry Petri dish at room conditions;
- Incubate treatment: the coupon was incubated in a Petri dish on B4 Succinate media without glucose (2 g/L yeast extract, 2.5 g/L calcium succinate) at room conditions for 1 week;
- Damage and repaint treatment: the coupon was cut parallel to the long axis, and then wet paint was used to try to “glue” the coupon back together; the coupon was stored in a clean, dry Petri dish at room conditions;
- Damage and regrow treatment: the coupon was cut parallel to the long axis, and then incubated in a Petri dish on B4 Succinate media without glucose at room conditions for 1 week to allow for self-healing. The cut edges were placed next to each other, but not touching. After a week, if self-healing was observed, the film was peeled from the agar. Images of some of the healed samples follow in Figure 29.

Figure 29 . Images of two healed samples. The scale markers are 500 µm. Both images show the self-healed "scar" running from the edge of the coupon on the left to the right side of the image. The entire healed length was 1-1.5 cm, although only the edge of the scar is shown in the image. The Image on the right was back-lit to highlight the microbial growth that connects the two, and a black background was digitally added for contrast.

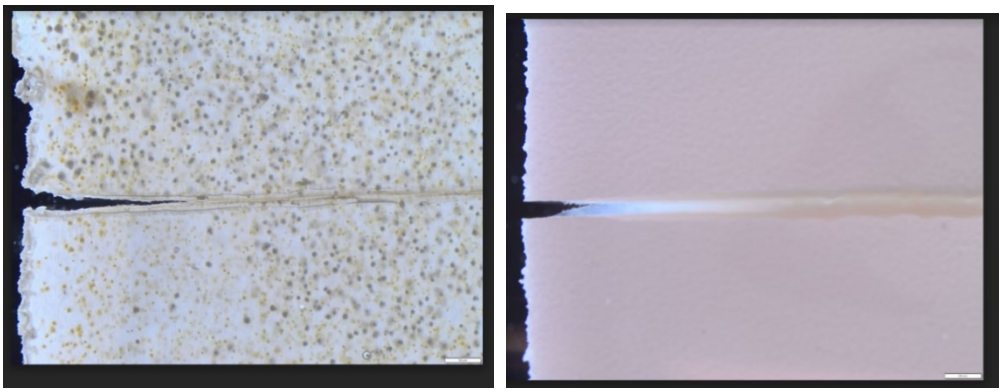

Most of the healed samples were robust to handling and did not break before testing; however, the PS2 samples (even the controls) could not be removed from the mat to test. As expected, the samples generally lost some strength from incubating on the agar for a week, with styrene-acrylic coating and the PS3 paint showing more sensitivity to incubation than the acrylic coatings**.** Since the self-healed samples also incubated on agar for a week, the incubated controls were the appropriate comparisons.

The cohesive strength was measured using a modified version of ASTM D882, "Standard Test Method for Tensile Properties of Thin Plastic Sheeting," which typically requires the use of an Instron tensile testing machine. Results of this test are described below.

The styrene-acrylic coating and PS3 paint had generally similar results. The self-healed samples retained 39% and 8.5% of the strength of the incubated comparison. The acrylic self-healed coatings with spores had strength similar to the control, and the acrylic coating with vegetative cells retained 19% of the strength of the incubated comparison.

Samples with spores could not be re-painted back together, so it is not possible to compare them to the microbially-healed samples. The styrene-acrylic and PS3 self-healed samples with vegetative cells were 58% stronger and 85% weaker, respectively, than the repainted versions. The acrylic self-healed sample with vegetative cells was 43% stronger than the repainted version.

Figure 30. Samples tested for strength. The scale bars are 1 mm. A) and B) are the same coating before and after testing.

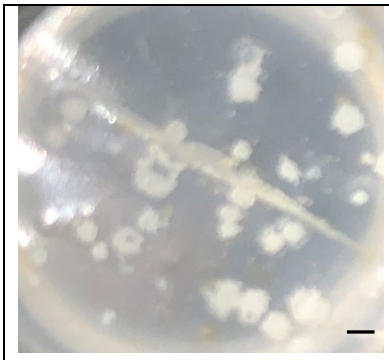	A) Sample coating before testing. The coupon was cut and allowed to incubate on B4 succinate minimal media for a week. On the left, the scar from self-healing can be seen running from the upper left to the lower right.
	B). Sample coating after testing. As expected, the healed portion that runs from left to right was the source of the cohesive failure.

A washability method based on ASTM D4824 – Standard Test Method for Washability of organic coatings was used to determine if a standard method that includes abrasion and wetting could be carried out on the Living Paint samples. Two test coatings (the styrene-acrylic and PS3) that contained no bacteria, vegetative P6A, P6A spores, or Comamonas 1 were drawn down on a Leneta Scrub Test Panel (P121-10N). At least 2 mil thick drawdowns of the paints were applied to the scrub panel and cured for 45 days (Figure 31, Left). The multiple drawdowns on the scrub panel were tested simultaneously. The panel was placed on a Gardco Washability Machine; 10 mL of water was placed on each drawdown (Figure 31, Right). An additional 10 mL of water was applied to a damp sponge and placed in the weighted sponge holder on the scrub machine. The panel was washed for 50 cycles. The coating was wet for approximately 15 minutes. After the test, the panel was removed from the scrub machine and rinsed with tap water. The panel was evaluated for any film failures that occurred during the wash. After the panel had dried for 10 days at room temperature and humidity, a final visual examination of the panel was completed.

No film failures were observed while washing or immediately afterward for any of the samples. No growth or additional calcium carbonate was noticed 10 days after the panels had dried. Microscopic evaluation of the panels indicated that the wetting and abrasion with a sponge was not sufficient to cause the microbes to grow.

Figure 31. Left side: PS3 Drawdowns containing *Comamonas 1* before washing, Right side: The same coatings loaded with 10 mL of water on each drawdown.

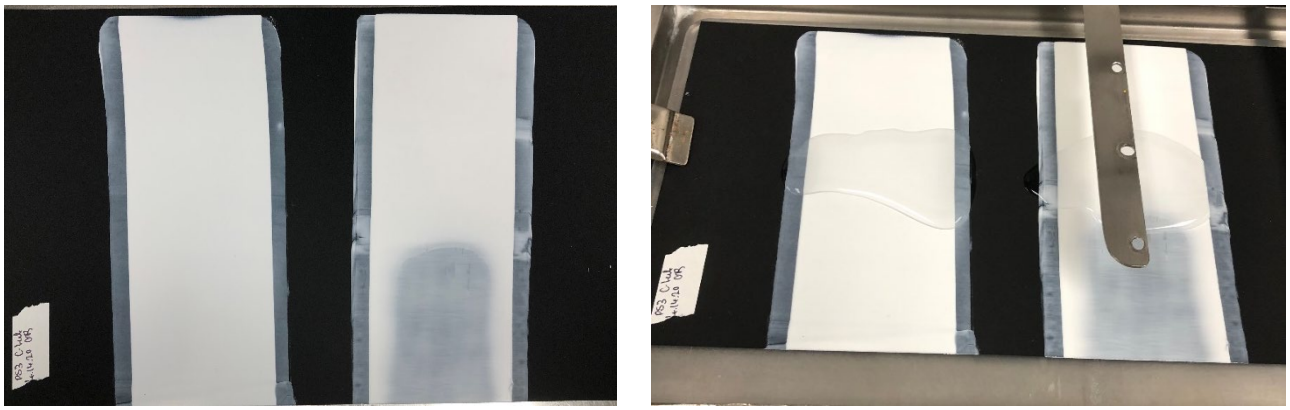

3.9.3 Important Findings and Conclusions

We were successfully able to test several Living Paint Samples with typical coatings methods. Many of the self-healed samples were surprisingly durable and could be easily handled without breaking. The self-healed samples were between 8% and 39% as durable as undamaged coupons that were incubated on agar for a comparable time. In at least one case, the undamaged coating failed before the self-healed portion, suggesting that microbially-induced self-healing is a route to healing without loss of coating strength.

The coatings were also able to withstand a typical washability test in which they were abraded with a sponge while wet. The washability test did not cause the microbes to grow or calcify, consistent with the results from Task 1 and Task 5, where continuous wetting was necessary to initiate growth and calcification. These results suggest that a self-healing paint system is capable of a practical level of performance.

4 Summary of Results and Implications for Further Research

The Living Paint Project demonstrated that the calcium toxicity mechanism may be harnessed to induce microbial precipitation of $CaCO_3$ in a coating system for self-healing. Unlike ureolytic approaches, this mechanism does not require the addition of urea to the coating. New mass and volume are created from the sequestration of atmospheric CO_2 which is converted to bicarbonate and then carbonate. When exposed to the appropriate calcium salts, many of our environmental pool microbes demonstrated this capability.

We have made substantial progress towards a successful self-healing system, demonstrating 10 x 0.25 x 0.25 mm^3 repair within a week that is visually opaque and close to our goal of 10 x 1 x 0.25 mm^3. Although a range of repair strengths were observed, at least one repair was stronger than the initial coating. The coatings were durable enough to withstand gentle scrubbing in a typical ASTM washability test, and the washability test did not unintentionally initiate microbial growth.

Efforts to provide fully autonomous control of the healing were less successful. This is one of the central difficulties of all chemically-actuated or “smart” systems: the system needs to be stable enough to prevent accidental or random actuation, unstable enough to be actuated, and be able to return to stability once the desired response had been demonstrated. In our systems, successful primary

actuators were water, nutrients, or a combination of both. In order to demonstrate a level of self-healing that met our program goals, samples needed to be in contact with an agar scaffold layer to provide nutrients and water. Although we were able to demonstrate some microbial growth and calcification in samples that had no growth media, those approaches required the manual application of water or liquid nutrient solutions to damaged areas to support microbial growth and calcification and resulted in only a small amount of growth. Future work addressing access to water and decoupling the activation of self-healing from the application of water is warranted. In practical systems, the coating may be subject to unpredictable amounts of rain and humidity.

Several of our approaches to enhance control relied on the ability to genetically-modify the functional microbes. In a model *E. coli* system, we increased the expression of a carbonic anhydrase and a divalent cation transporter protein. These transformations resulted in a calcification phenotype that was absent in the *E. coli* wildtype. Since the pool of functional microbes was chosen in part by demonstrating calcification, we hypothesized that overexpressing similar proteins would result in the hypersecretion of calcium carbonate. Increasing the rate of calcite production could result in the microbes entombing themselves in a shell of $CaCO_3$, which would act as an "off switch" to prevent further calcification and return the system to a stable state.

We successfully cloned multiple native genes into an expression plasmid and introduced them into two wild *Comamonas* strains. The *Comamonas* is Gram negative and proved to be good candidates for transformation. Although expression of the carbonic anhydrase in *Comamonas 1* increased calcium carbonate formation in liquid cultures, these results did not translate to solid media. The overexpression of a divalent cation exporter did not affect calcification. However, ion transport proteins may be specific to a strain; further work may be needed to identify one that increases calcification. No homolog to the *zntB* gene, which increased calcification when overexpressed in *E. coli,* was identified in either Comamonas strain. Multiple transporters will need to be screened to identify one that works to export calcium.

The tractability of Gram negative species to transformation makes them appealing candidates for self-healing coatings. However, the Gram negative species were generally not able to survive in liquid coating formulas. Only a few were capable of growth and calcification after drying into a paint film, and only in the first few days. Initial work on encapsulation strategies for Gram negative species was promising, increasing their lifetime in liquid paint formulas to a month, and further enhancement of the durability of Gram negative species to desiccation is a promising area for further work.

Some of the Gram positive microbes were spore-formers, and this was shown to successfully protect the microbes in liquid coating formulas for over four months. When dried into a coupon, the spores were capable of germination, growth, calcification, and crack filling when actuated, even after six months of room temperature storage. A genetic system was not stably integrated into either of the *Bacillus* strains. Further work on genetic modification of Gram positive species might allow for systems that capitalize on the compatibility of spore formers with coatings material.

[i] Ehrlich, H.L. and D.K. Newman, *Geomicrobiology*. 5th ed. 2008, Boca Raton, FL: CRC Press. 628.
[ii] Zhu T, Dittrich M. Carbonate precipitation through microbial activities in natural environment, and their potential in biotechnology: a review. Frontiers in bioengineering and biotechnology. 2016;4.
And Ehrlich, H.L. and D.K. Newman, *Geomicrobiology*. 5th ed. 2008, Boca Raton, FL: CRC Press. 628.
[iii] Altermann W, Kazmierczak J, Oren A, Wright DT (2006) Cyanobacterial calcification and its rock-building potential during 3.5 billion years of Earth history. *Geobiology* **4**, 147–166.
[iv] Banks E.D., Taylor N.M., Gulley J., Lubbers B.R., Giarrizzo J.G., Bullen H.A., Hoehler T.M. & Barton H.A., 2010 - Bacterial calcium carbonate precipitation in cave environments: a function of calcium homeostasis. Geomicrobiology Journal, 27: 444-454
[v] KV Tittelboom, N De Belie, W De Muynck, W Verstraete 2010 Use of bacteria to repair cracks in concrete. Cement and Concrete Research 40:157-166.
[vi]Jonkers, HM. 2011. Bacteria-based self healing concrete. HERON Vol 56, No. 1/2.
[vii] BOQUET E, BORONAT A, RAMOS-CORMENZANA A. 1973. Production of Calcite (Calcium Carbonate) Crystals by Soil Bacteria is a General Phenomenon. Nature 246:527–529.
SHEU, T. Y., & MARSHALL, R. T. (1993). *Microentrapment of Lactobacilli in Calcium Alginate Gels. Journal of Food Science, 58(3), 557–561.* [viii]
[ix] Banks E.D., Taylor N.M., Gulley J., Lubbers B.R., Giarrizzo J.G., Bullen H.A., Hoehler T.M. & Barton H.A., 2010 - Bacterial calcium carbonate precipitation in cave environments: a function of calcium homeostasis. Geomicrobiology Journal, 27: 444-454
[x] Barton H., unpublished results.
[xi]Legland, D., I. Arganda-Carreras, and P. Andrey, MorphoLibJ: integrated library and plugins for mathematical morphology with ImageJ. Bioinformatics, 2016. 32(22): p. 3532-3534.
[xii] Schneider, C.A., W.S. Rasband, and K.W. Eliceiri, NIH Image to ImageJ: 25 years of image analysis. Nature methods, 2012. 9(7): p. 671-675